

AD-A054 532

CALIFORNIA INST OF TECH PASADENA GUGGENHEIM JET PROP--ETC F/G 20/4  
MEASUREMENTS OF ENERGY LOSSES ASSOCIATED WITH INTERACTIONS BETW--ETC(U)  
MAR 78 F E CULICK, K MAGIAWALA F04611-75-C-0010

UNCLASSIFIED

AFRPL-TR-78-6

NL

| OF |  
AD  
A054532



END  
DATE  
FILMED  
6-78  
DDC

AD A054532

FOR FURTHER TRAN

18  
19  
AFRPL TR-78-6

See AD A029165

6 MEASUREMENTS OF ENERGY LOSSES ASSOCIATED WITH INTERACTIONS BETWEEN ACOUSTIC WAVES AND A STEADY FLOW FIELD,

Daniel and Florence Guggenheim Jet Propulsion Center  
California Institute of Technology  
Pasadena, California 91125

10  
Authors: F. E. C./Culick/ Professor of Engineering  
K./Magiawala/ Research Assistant

11 15 Mar 78

12 8 P.P.

Final Report, 16 Mar 76 — 15 Nov 77.

9 15 4611-75-C-4P14

16 573P

17 1P

APPROVED FOR PUBLIC RELEASE;

DISTRIBUTION UNLIMITED

AD No. 1  
DDC FILE COPY

AIR FORCE ROCKET PROPULSION LABORATORY  
DIRECTOR OF SCIENCE AND TECHNOLOGY  
AIR FORCE SYSTEMS COMMAND  
EDWARDS AFB, CALIFORNIA 93523

DDC  
JUN 2 1978  
F

159 600

mt

## NOTICES

When U.S. Government drawings, specifications, or other data are used for any purpose other than a definitely related government procurement operation, the Government thereby incurs no responsibility nor any obligation whatsoever, and the fact that the Government may have formulated, furnished, or in any way supplied the said drawings, specifications or other data, is not to be regarded by implication or otherwise, or in any manner licensing the holder or any other person or corporation, or conveying any rights or permission to manufacture use, or sell any patented invention that may in any way be related thereto.

## FOREWORD

This report was submitted by Daniel and Florence Guggenheim Jet Propulsion Center, California Institute of Technology, Pasadena, California 91125, under Contract No. F04611-75-C-0010, Job Order No. 573010AU with the Air Force Rocket Propulsion Laboratory, Edwards AFB, California 93523.

The authors wish to express their appreciation to personnel in the Solid Propellant Section, the Standards and Calibrations Laboratory and the Environmental Testing Laboratory, all of the Jet Propulsion Laboratory. Without their advice and assistance, including loan of equipment, the performance of the work reported here would have been inestimably more difficult.

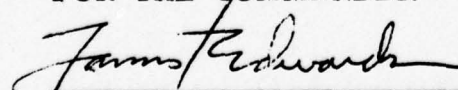
This report has been reviewed by the Information Office/DOZ and is releaseable to the National Technical Information Service (NTIS). At NTIS it will be available to the general public, including foreign nations.

This report is unclassified and suitable for general public release.

  
Jay N. Levine  
Project Engineer

  
W. C. Andrepont, Chief  
Combustion Group

FOR THE COMMANDER

  
John I. Washburn, Major USAF,  
Chief, Propulsion Analysis Division



UNCLASSIFIED

SECURITY CLASSIFICATION OF THIS PAGE (When Data Entered)

REPORT DOCUMENTATION PAGE		READ INSTRUCTIONS BEFORE COMPLETING FORM
1. REPORT NUMBER AFRPL-TR-78-6 ✓	2. GOVT ACCESSION NO.	3. REPORT'S CATALOG NUMBER
4. TITLE (and Subtitle) MEASUREMENTS OF ENERGY LOSSES ASSOCIATED WITH INTERACTIONS BETWEEN ACOUSTIC WAVES AND A STEADY FLOW FIELD		5. TYPE OF REPORT & PERIOD COVERED Final Report 16 Mar. 1976-15 Nov. 1977
7. AUTHOR(s) F.E.C. Culick K. Magiawala		6. PERFORMING ORG. REPORT NUMBER
9. PERFORMING ORGANIZATION NAME AND ADDRESS Daniel and Florence Guggenheim Jet Propulsion Center, California Institute of Technology, Pasadena, California 91125		8. CONTRACT OR GRANT NUMBER(s) F04611-75-C-0010
11. CONTROLLING OFFICE NAME AND ADDRESS Air Force Rocket Propulsion Laboratory/PAC Director of Science and Technology Air Force Systems Command Edwards AFB, California 93523		10. PROGRAM ELEMENT, PROJECT, TASK AREA & WORK UNIT NUMBERS JON 573010AU
14. MONITORING AGENCY NAME & ADDRESS (if different from Controlling Office)		12. REPORT DATE 15 March 1978
		13. NUMBER OF PAGES 78
		15. SECURITY CLASS. (of this report) Unclassified
		15a. DECLASSIFICATION/DOWNGRADING SCHEDULE
16. DISTRIBUTION STATEMENT (of this Report) Approved for Public Release; Distribution Unlimited		
17. DISTRIBUTION STATEMENT (of the abstract entered in Block 20, if different from Report)		
18. SUPPLEMENTARY NOTES		
19. KEY WORDS (Continue on reverse side if necessary and identify by block number) Combustion Instability T-Burners Acoustics Solid Propellant Rockets 62302F		
20. ABSTRACT (Continue on reverse side if necessary and identify by block number) ✓ An experimental program has been conducted to study interactions between acoustic waves and non-uniform flow fields. Data have been taken in an impedance tube, modified to accommodate an average flow, and in a resonance tube. Results are given for the influence of flow through a subsonic exhaust vent on an acoustic field. Measurements for circular and slot vents of several sizes and for two frequencies show that the flow through the vent causes a transfer of energy from the average flow field to the acoustic field; The vent acts as a source		

DDC  
JUN 2 1978  
RECEIVED  
F

UNCLASSIFIED

SECURITY CLASSIFICATION OF THIS PAGE (When Data Entered)



UNCLASSIFIED

SECURITY CLASSIFICATION OF THIS PAGE(When Data Entered)

Block 20 (continued) Abstract

or gain of acoustic energy.

ACCESSION for	
NTIS	<input checked="" type="checkbox"/>
DDC	<input type="checkbox"/>
UNANNOUNCED	<input type="checkbox"/>
JUSTIFICATION	
BY	
DISTRIBUTION/AVAILABILITY	
Dist.	Av.
<input checked="" type="checkbox"/>	<input type="checkbox"/>

UNCLASSIFIED

SECURITY CLASSIFICATION OF THIS PAGE(When Data Entered)

## TABLE OF CONTENTS

	<u>Page No.</u>
I. INTRODUCTION	10
II. ANALYSIS OF THE APPARATUS FOR ACOUSTICS TESTS	13
2.1 Analysis of the Resonance Tube	13
2.2 Analysis of the Impedance Tube	18
III. DESCRIPTION OF APPARATUS AND INSTRUMENTATION	22
3.1 Resonance Tubes	22
3.2 Impedance Tube	28
IV. CALIBRATION PROCEDURES AND ESTIMATES OF ERRORS	31
4.1 Calibration of the Gas Supply System	31
4.2 Calibration of Microphones	34
4.3 Sources and Estimates of Errors	34
V. MEASUREMENTS OF THE ADMITTANCE FUNCTION FOR THE POROUS PLATES	38
VI. MEASUREMENTS OF THE NET ACOUSTIC LOSSES IN THE RESONANCE TUBES	45
VII. ANALYSIS OF THE RESULTS AND DETERMINATION OF THE INFLUENCE OF AN EXHAUST VENT	59
7.1 The Influence of a Vent According to the One-Dimensional Approximation	59
7.2 Determination of Radiation Losses Through the Vent	60
7.3 Internal Consistency of the Data and Losses Through the Lateral Boundary	62
7.4 Determination of the Attenuation Constant for the Exhaust Vents	65
VIII. CONCLUDING REMARKS	75

# Table of Contents (cont.)

	Page No.
INTRODUCTION	77
II. ANALYSIS OF THE APPARATUS FOR ACOUSTICS TESTS	
2.1 Analysis of the Resonance Tube	78
2.2 Analysis of the Impedance Tube	79
III. DESCRIPTION OF APPARATUS AND INSTRUMENTATION	
3.1 Resonance Tubes	81
3.2 Impedance Tube	82
IV. CALIBRATION PROCEDURES AND ESTIMATES OF ERRORS	
4.1 Calibration of the Gas Supply System	83
4.2 Calibration of Microphones	84
4.3 Sensors and Estimates of Errors	85
V. MEASUREMENTS OF THE ADMITTANCE FUNCTION FOR THE POROUS PLATES	
VI. MEASUREMENTS OF THE NET ACOUSTIC LOSSES IN THE RESONANCE TUBES	
VI. ANALYSIS OF THE RESULTS AND DETERMINATION OF THE INFLUENCE OF A. EXHAUST VELOCITY	
6.1 The Influence of a Vent According to the One-Dimensional Approximation	86
6.2 Determination of Radiation Losses Through the Vent	87
6.3 Internal Consistency of the Data and Losses Through the Lateral Boundary	88
6.4 Determination of the Absorption Coefficient for the Exhaust Vents	89
VII. CONCLUDING REMARKS	90



# LIST OF SYMBOLS

$a_o$	speed of sound
$A_b$	admittance function for the porous plates
$D$	diameter of resonance or impedance tube
$D_{nn}$	damping constant, Equation (6)
$\mathcal{E}$	acoustic energy density
$E_n^2$	$E_n^2 = \int \psi_n^2 dV$
$E_{nn}$	constant appearing in Equation (6)
$f$	frequency; also used for right hand side of Equation (2)
$F_n$	forcing function, Equation (4)
$G$	defined by Equation (11)
$h$	right hand side of Equation (1)
$L$	length of resonance tube
$\bar{M}$	average Mach number
$p_o$	average pressure
$p'$	pressure fluctuation
$R$	defined by Equation (12)
$S_b$	area of burning surface or of porous plates
$S_c$	cross-section area of resonance tube
$dS$	element of area
$t$	time
$\vec{u}_p, u_p$	velocity of piston
$dV$	element of volume
$\alpha$	attenuation constant
$\alpha_o$	defined by Equation (14)

$\alpha_b$	attenuation constant associated with $A_b$
$\alpha_d$	attenuation constant for radiation and viscous losses
$\alpha_v$	attenuation constant for the exhaust vent
$\alpha_{net}$	net measured attenuation constant, Equation (18)
$\beta_o$	defined by Equation (15)
$\gamma$	ratio of specific heats
$\eta_n$	amplitude of the $n^{th}$ mode
$\kappa$	defined by Equation (13)
$\sigma$	standard deviation
$\psi_n$	mode shape for the $n^{th}$ mode
$\omega_n$	resonant frequency of the $n^{th}$ mode
$\tilde{\omega}_n$	defined by Equation (9)
$\nu$	kinematic viscosity
$( )^{(r)}$	real part
$( )^{(i)}$	imaginary part
$(\bar{\quad})$	statistical average
$(\hat{\quad})$	amplitude, $\phi = \hat{\phi} \exp(i\omega t)$
$(\dot{\quad})$	time derivative
$\Delta(\quad)$	standard deviation
$\langle \rangle$	time average

## LIST OF FIGURES

<u>Figure Number</u>		<u>Page No.</u>
1.	Sketch of a Resonance Tube	14
2.	Resonance Curve According to Equation (8)	15
3.	Sketch of the Impedance Tube	19
4.	Schematic Diagram of the Resonance Tube and Apparatus	23
5.	Details of the Piston	24
6.	Anechoic Chamber Floor Plan Showing Location of Apparatus	27
7.	Schematic Diagram of Impedance Tube and Apparatus	29
8.	Flow Circuit for Calibration of Porous Plates	32
9.	Data for Flow Rates Through the Porous Plates	33
10.	Measured Admittance Functions at 442.70 Hz.	43
11.	Measured Admittance Functions at 1345.00 Hz.	44
12.	Net Values of Attenuation Constant, 1/2 Inch Circular Vent, 442.70 Hz.	53
13.	Net Values of Attenuation Constant, 1 Inch Vent, 444.79 Hz.	54
14.	Net Values of Attenuation Constant, 1 1/2 Inch Vent, 451.61 Hz.	55
15.	Net Values of Attenuation Constant, 0.167 Inch Slot Vent, 446.72 Hz.	56
16.	Net Values of Attenuation Constant, 0.375 Inch Slot Vent, 446.09 Hz.	57
17.	Net Values of Attenuation Constant, 1/2 Inch Circular Vent, 1340.88 Hz.	58
18.	Attenuation Constant for the 1/2 Inch Circular Vent, 442.70 Hz.	71



# LIST OF FIGURES (continued)

<u>Figure Number</u>		<u>Page No.</u>
19.	Attenuation Constant for the 1 Inch Circular Vent, 442.70 Hz.	72
20.	Attenuation Constant for the 1 1/2 Inch Circular Vent, 442.70 Hz.	73
21.	Attenuation Constant for the 1/2 Inch Circular Vent, 1345.00 Hz.	74

# LIST OF TABLES

<u>Table Number</u>		<u>Page No.</u>
1.	Data Taken With Impedance Tube, Porous Plate #1, Frequency 442.7 Hz.	39
2.	Data Taken With Impedance Tube, Porous Plate #2, Frequency = 442.70 Hz.	40
3.	Data Taken With Impedance Tube, Porous Plate #1, Frequency = 1345 Hz.	41
4.	Data Taken With Impedance Tube, Porous Plate #2, Frequency = 1345 Hz.	42
5.	Data Taken With Resonance Tube, $\frac{1}{2}$ " Circular Vent, Frequency = 442.70 Hz.	47
6.	Data Taken With Resonance Tube, 1" Circular Vent, Frequency = 444.79 Hz.	48
7.	Data Taken With Resonance Tube, $1\frac{1}{2}$ " Circular Vent, Frequency = 451.61 Hz.	49
8.	Data Taken With Resonance Tube, 1" Eq Slot Vent, Frequency = 446.72 Hz.	50
9.	Data Taken With Resonance Tube, $1\frac{1}{2}$ " Eq Slot Vent, Frequency = 446.09 Hz.	51
10.	Data Taken With Resonance Tube, $\frac{1}{2}$ " Circular Vent, Frequency = 1340.88 Hz.	52
11.	Attenuation Constant Due to Radiation of Acoustic Energy From Circular Exhaust Vents	61
12.	Verification of the Data For Circular Vents With No Flow. (Vent Closed) Frequency = 442.70 Hz.	64
13.	Values of the Average Attenuation Constant and Standard Deviation for Three Circular Vents. (Frequency = 442.7 Hz.)	69
14.	Slopes and Standard Deviation of the Attenuation Constant for Five Exhaust Vents. (Frequency = 442.7 Hz.)	70

## I. INTRODUCTION

Significant influences on the behavior of acoustic waves arise when the waves propagate in non-uniform average flow fields. Special cases occur in regions where the average flow enters or leaves a chamber in which acoustic waves are excited. A particularly important situation is encountered in devices for testing the dynamical behavior of solid propellants, when the average flow enters or leaves in directions not parallel to the acoustical motions. Several years ago, an approximate analysis first suggested that in such situations energy is exchanged between the average and unsteady fields. When the average flow leaves the chamber, energy is transferred to the acoustic field, a phenomenon sometimes referred to as the "vent gain."

Although that prediction is a correct conclusion of the one-dimensional analysis (Refs. 2 and 3), it is at least unanticipated, and could be invalid because of the approximations involved. The issue is an important one to settle owing to its significance for the treatment of data taken with T-burners (Ref. 4, for example). If the exhaust vent provides a gain of acoustic energy, then the values deduced for the response function of a burning propellant are lower

- 
1. Culick, F.E.C. and Magiawala, K., "Measurements of Energy Losses Associated With Interactions Between Acoustic Waves and a Steady Flow Field," Final Report, Contract No. F04611-75 C-0010, AFRPL Report TR-76.
  2. Culick, F.E.C., "The Stability of One-Dimensional Motions in a Rocket Motor," Comb. Sci. and Tech., V. 7 (1973), pp. 165-175.
  3. Culick, F.E.C., "Remarks on Entropy Production in the One-Dimensional Approximation to Unsteady Flow in Combustion Chambers," Comb. Sci. and Tech., V. 15 (1977), pp. 93-97.
  4. Culick, F.E.C. (Ed.), "T-Burner Testing of Metallized Propellants," AFRPL Report TR-74-28 (Oct. 1974).



than those inferred when the vent is assumed to have no effect, or to cause a loss of acoustic energy.

Experimental work described in this report has been directed to determining the influence of a subsonic exhaust vent in the lateral boundary of a T-burner. All tests have been conducted with air at room temperature, to eliminate the uncertainties associated with combustion processes. Two sorts of experiments have been performed: tests in an impedance tube to measure the admittance function for porous pistons used to drive the waves; and tests in a resonance tube to determine the losses or gains associated with the vent.

The results obtained here show that indeed a subsonic exhaust vent in the lateral boundary does produce a gain of acoustic energy. Data have been taken for both circular and slot vents located at the center of a tube, a configuration similar to the T-burner. The fundamental longitudinal acoustic mode is driven by oscillating pistons at the ends. Average flow is introduced through the porous faces of the pistons and exhausts through the vent at the center. The main tube has an internal diameter of one and one-half inches; most of the measurements have been taken in a tube fifteen inches long, the fundamental frequency being 442 Hz. Five different vents have been used: one-half, one, and one and one-half inch circular vents; and annular slot vents having the same areas as the one, and one and one-half inch circular vents. One series of tests has been performed at 1350 Hz. with the one-half inch circular vent.

In all cases, the average Mach number of the average flow in the main chamber has been varied from zero to 0.0022. This

includes the range in which most T-burner tests are performed. For all the conditions examined, the gain of acoustic energy increases with the Mach number, approximately linearly.

Thus we have been able to check three aspects of the prediction based on the one-dimensional approximation: (i) for a fixed total flow rate, the gain of energy is independent of the cross-section area and the shape of the vent; (ii) the gain of energy increases linearly with the Mach number of the average flow; (iii) the gain of energy is proportional to the frequency. All of the data fall within 30% of the values predicted with the one-dimensional analysis. There seems little doubt at this time that the approximate analysis does represent quite well the dominant effects of mean flow/acoustics interactions for a subsonic vent in the lateral boundary of a resonance tube.

The amount of analysis required in this work is minimal and has been covered thoroughly in Ref. 1. Here in § II a brief summary is given for both the resonance tube and the impedance tube. The apparatus and instrumentation are described in § III. Crucial items are the calibration of the measuring devices and estimates of the errors, discussed in § IV. The admittance functions of the porous plates through which the mean flow is introduced must be measured independently. This has been done using the impedance tube; the results are given in § V. The measurements taken with the resonance tube are summarized in § VI and the final results for the influence of the vent are discussed in § VII.

## II. ANALYSIS OF THE APPARATUS FOR ACOUSTICS TESTS

Because this subject was covered quite thoroughly in Reference 1, there is no need here to provide a complete discussion. For later reference in this report it is useful to quote the main results.

There are two devices required to produce the results we seek: a resonance tube with provision for average flow; and an impedance tube, also designed to accommodate average flow. The analyses are relatively straight forward but crucial to the work because the quantities eventually of interest cannot be measured directly. Determination of the influence of the vent rests on a combination of experimental data and analysis.

### 2.1 Analysis of the Resonance Tube

The resonance tube is shown in Figure 1. In all the tests reported here it is driven by the oscillating pistons, in its fundamental mode: the pressure fluctuation is maximum at the ends and has a node at the center. When the frequency of the driving mechanism is swept through the resonant frequency, the amplitude of the pressure oscillation varies as shown in Figure 2. Thus, the behavior appears to be very much like that of a simple spring/mass/dashpot system. The purpose of the analysis is to establish the correct representation. In particular, we need to relate the width of the resonance curve to the net losses in the system.

From the conservation equations, a linear inhomogeneous wave equation can be constructed for the pressure oscillations,



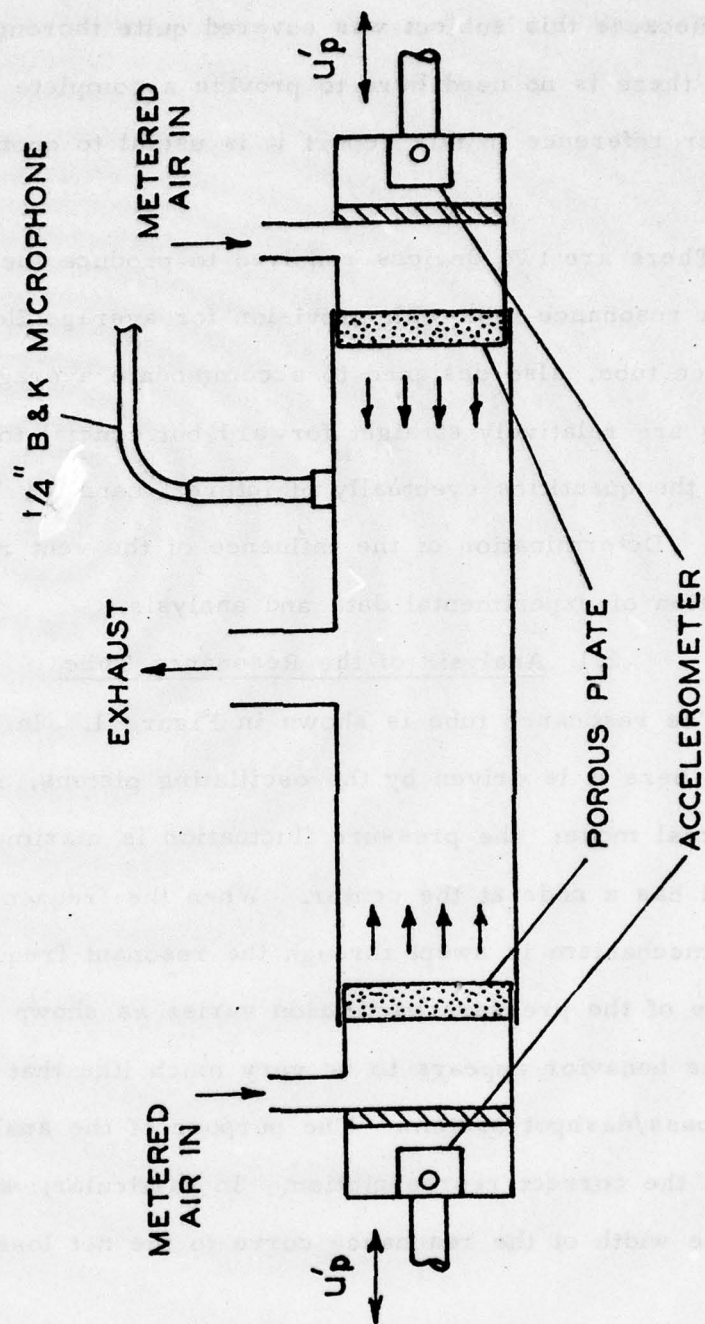
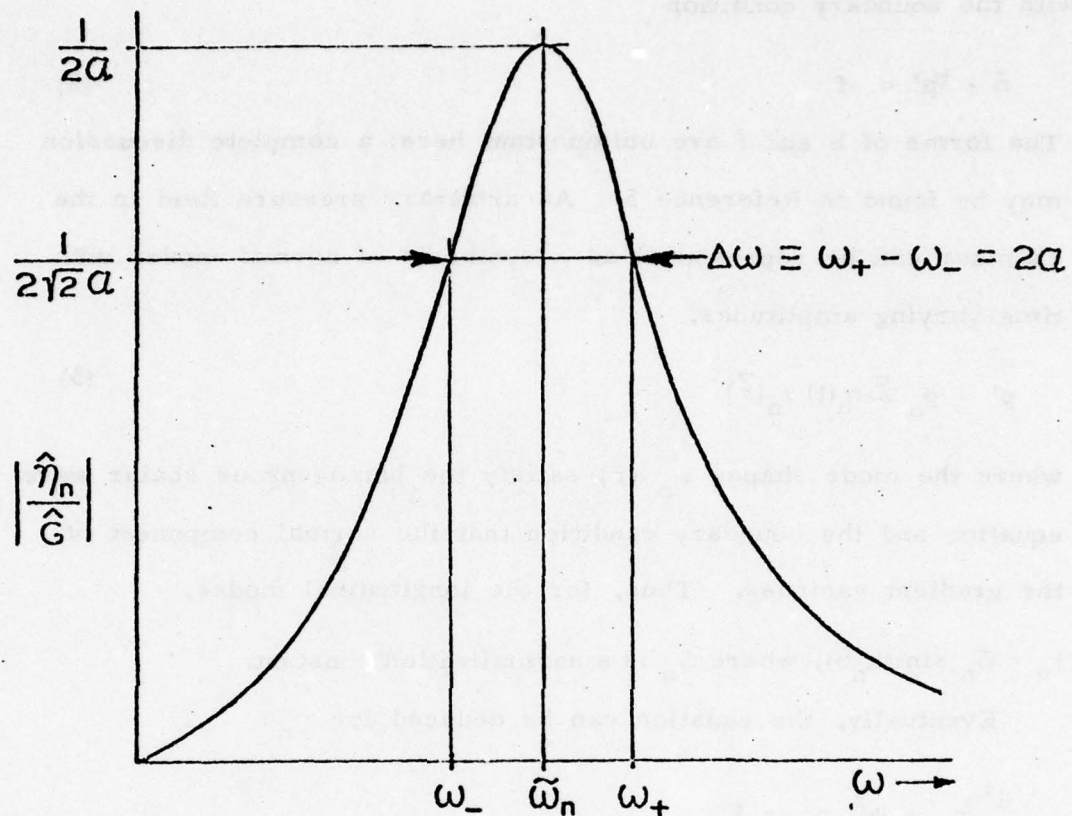


Figure 1. Sketch of a Resonance Tube



**Figure 2.** Resonance Curve  
According to Equation (8)

$$\nabla^2 p' - \frac{1}{a_o^2} \frac{\partial^2 p'}{\partial t^2} = h \quad (1)$$

with the boundary condition

$$\hat{n} \cdot \nabla p' = -f \quad (2)$$

The forms of  $h$  and  $f$  are unimportant here; a complete discussion may be found in Reference 5. An arbitrary pressure field in the chamber can be represented as a synthesis of normal modes with time-varying amplitudes,

$$p' = p_o \sum \eta_n(t) \psi_n(\vec{r}) \quad (3)$$

where the mode shapes  $\psi_n(\vec{r})$  satisfy the homogeneous scalar wave equation and the boundary condition that the normal component of the gradient vanishes. Thus, for the longitudinal modes,

$\psi_n = C_n \sin(k_n z)$ , where  $C_n$  is a normalization constant.

Eventually, the equation can be deduced for  $\eta_n$ :

$$\frac{d^2 \eta_n}{dt^2} + \omega_n^2 \eta_n = F_n \quad (4)$$

with

$$F_n = - \frac{a_o^2}{p_o \int \psi_n^2 dV} \left\{ \int \psi_n h dV + \oint \psi_n f dS \right\} \quad (5)$$

- 
5. Culick, F.E.C. "Nonlinear Behavior of Acoustic Waves in Combustion Chambers" Daniel and Florence Guggenheim Jet Propulsion Center, California Institute of Technology, Pasadena, Calif. (April 1975)



Part of the forcing function  $F_n$  depends on  $\eta_n$ , while part represents the externally controlled driving. Equation (4) may be rearranged in the form

$$\frac{d^2 \eta_n}{dt^2} + \left[ D_{nn} + \frac{2a_o A_b^{(r)} S_c}{E_n^2} \right] \frac{d\eta_n}{dt} + \left[ \tilde{\omega}_n^2 + E_{nn} - \frac{2a_o \omega_n A_b^{(i)} S_c}{E_n^2} \right] \eta_n = - \frac{\gamma}{E_n^2} \oint \psi_n \frac{\partial \vec{u}_p}{\partial t} \cdot \hat{n} dS. \quad (6)$$

This equation is the formal justification for the very simple and appealing view that the system (the resonance tube) behaves as a driven oscillator whose "displacement" is the amplitude  $\eta_n$  of the mode being driven. The piston is forced harmonically with velocity parallel to the axis of the tube,  $\vec{u}_p = \vec{u}_p \cdot \hat{n}$  and

$$\vec{u}_p = \hat{u}_p e^{i\omega t} \quad (7)$$

With  $\eta_n = \hat{\eta}_n \exp(i\omega t)$ , Equation (6) leads to the frequency response

$$\hat{\eta}_n = \frac{-i\omega \hat{G}}{(\tilde{\omega}_n^2 - \omega^2) + i\omega(2\alpha)} \quad (8)$$

where

$$\tilde{\omega}_n^2 = \omega_n^2 + E_{nn} - \frac{2a_o \omega_n A_b^{(i)} S_c}{E_n^2} \quad (9)$$

$$2\alpha = \frac{D_{nn} + 2a_o A_b^{(r)} S_c}{E_n^2} \quad (10)$$

$$\hat{G} = -\frac{\gamma}{E_n^2} \oint \hat{\psi}_n \hat{u}_p dS \quad (11)$$

The surface integral in  $\hat{G}$  extends over the faces of the pistons.

Several points are important to note:

1) As shown in Reference 1, the admittance  $A_b$  =  $A_b^{(r)} + iA_b^{(i)}$  is for the surface of a stationary piston. This is the quantity to be measured with the impedance tube.

2) As shown in Figure 2, the resonance curve has width  $2\alpha$  at the half-power points, for  $\alpha / \omega \ll 1$ . This is the basis for the measurements: the frequencies  $\tilde{\omega}_n$ ,  $\omega_+$ , and  $\omega_-$  are measured, and from the width  $\Delta\omega = \omega_+ - \omega_-$ , the contributions to  $\alpha$  given by (10) can be found.

3) The constant  $D_{nn}$  represents the influences of all losses in the system except those at the faces of the pistons. Determination of the influence of the vent requires subtraction of the values of  $\alpha$  (and hence  $D_{nn}$ ) found for different configurations. To achieve acceptable precision, the values of  $\alpha$  must be very accurately measured. This is the origin of the need for great care in performing the experiments.

## 2.2 Analysis of the Impedance Tube

The impedance tube is shown in Figure 3. In accord with remark (1) above, the piston to be tested is rigidly mounted, stationary with respect to the tube itself. Because the Mach number of the average flow is so small ( $\bar{M} < 5 \times 10^{-3}$ ), the standard

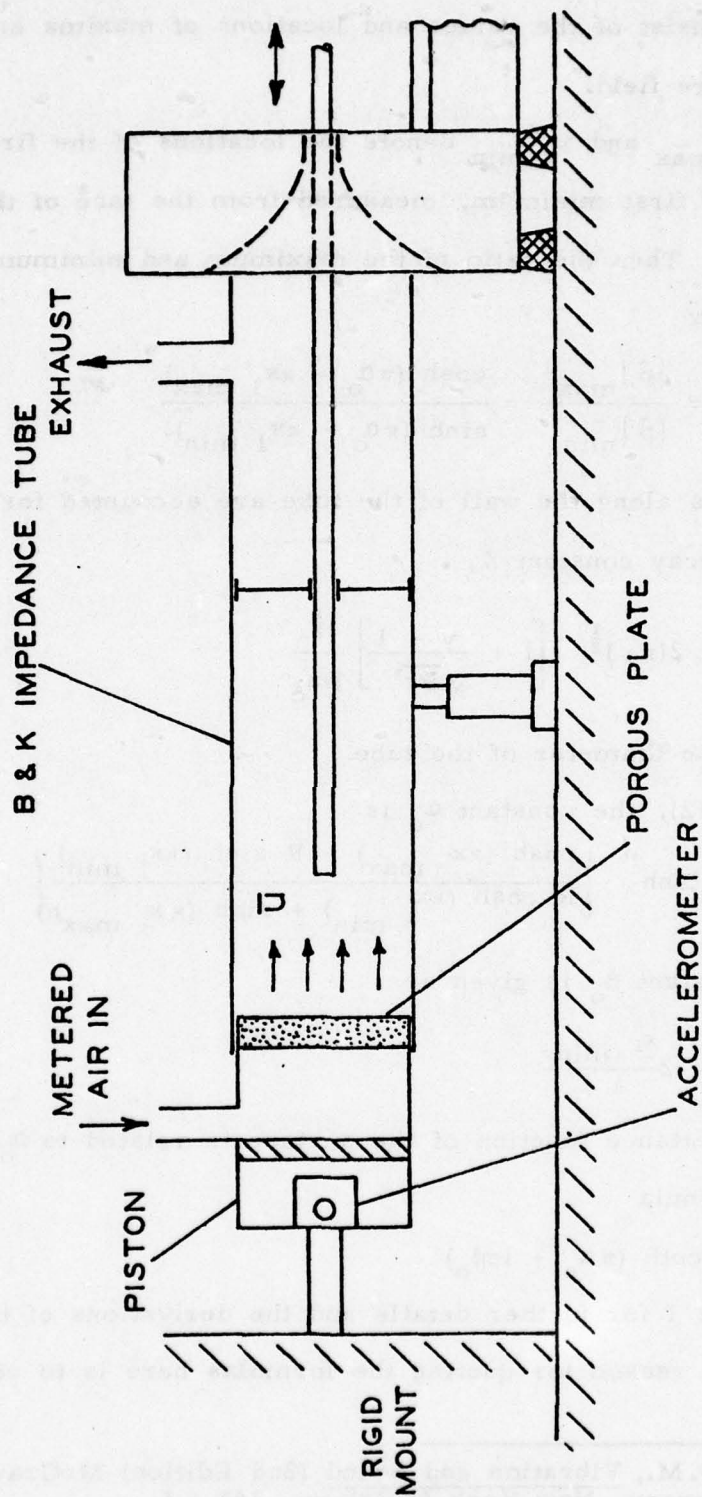


Figure 3. Sketch of the Impedance Tube



analysis of the impedance tube may be used. (Ref. 6) The measurements consist of the values and locations of maxima and minima of the pressure field.

Let  $x_{1 \max}$  and  $x_{1 \min}$  denote the locations of the first maximum and first minimum, measured from the face of the piston being tested. Then the ratio of the maximum and minimum values,  $R$ , is given by

$$R = \frac{|\hat{p}|_{\max}}{|\hat{p}|_{\min}} = \frac{\cosh(\pi \alpha_o - \kappa x_{1 \max})}{\sinh(\pi \alpha_o - \kappa x_{1 \min})} \quad (12)$$

Viscous losses along the wall of the tube are accounted for with the spacial decay constant  $\kappa$ ,

$$\kappa = 2(\pi \nu)^{\frac{1}{2}} \left[ 1 + \frac{\gamma - 1}{\sqrt{\text{Pr}}} \right] \frac{f^{\frac{1}{2}}}{\text{Da}_o} \quad (13)$$

where  $D$  is the diameter of the tube.

From (12), the constant  $\alpha_o$  is

$$\alpha_o = \frac{1}{\pi} \tanh^{-1} \left\{ \frac{\cosh(\kappa x_{1 \max}) - R \sinh(\kappa x_{1 \min})}{R \cosh(\kappa x_{1 \min}) + \sinh(\kappa x_{1 \max})} \right\} \quad (14)$$

A second constant  $\beta_o$  is given as

$$\beta_o = 1 - 2 \frac{x_{1 \min}}{\lambda} \quad (15)$$

Then the admittance function of the surface is related to  $\alpha_o$  and  $\beta_o$  by the formula

$$A_b = -\coth(\pi \alpha_o + i\pi \beta_o) \quad (16)$$

See Reference 1 for further details and the derivations of these results. One reason for quoting the formulas here is to correct

---

6. Morse, P.M., Vibration and Sound (2nd Edition) McGraw-Hill Book Company, New York (1948), pp. 242 f.f.

### III. DESCRIPTION OF APPARATUS AND EXPERIMENTATION

some errors in Equations (3.5), (3.18) and (3.19) of Reference 1, which are here correctly shown as (13), (12), and (14) respectively.

Virtually all of the apparatus and instrumentation have been

proposed since the tests reported in Reference 1. Figure 4

shows the equipment used with the resonance tube. The tube itself

is made of brass, having 1.81 cm I.D., 0.112 cm wall thick-

ness and for the tests at 440 Hz, the length is 32.42 cm. The

three circular endplate vents are of brass, having 0.3172 cm wall

thickness, and I.D. 1.17 cm, 1.24 cm, and 1.81 cm (W1, W2, and

W3, and 1.167, respectively). All are 3.30 cm long. Each has a

plug, machined so that when inserted the vent is closed by a

resonance exactly fitting the inside surface of the tube resonance

tube.

These endplate vents were constructed so that the pressure

static pressure equal to the static of the endplate vents having

I.D. 1.24 and 1.81 cm. It is to be noted that the vent were not

used, so that, as later remarks will show, the dynamic values

of the resonance constants associated with these two vents could

not be determined.

A particularly difficult problem to overcome was the testing

and accurate operation of the piston. It appeared that during the

first portion of this work a major source of error and noise

reproducibility of the data, was due to slippage of the piston

positions at the piston. We could not find a suitable piston for

measure accurately the position of the piston. Small displacements

means cause measurable changes in the resonant frequency of the

### III. DESCRIPTION OF APPARATUS AND INSTRUMENTATION

#### 3.1 Resonance Tubes

Virtually all of the apparatus and instrumentation have been improved since the tests reported in Reference 1. Figure 4 shows the equipment used with the resonance tube. The tube itself is made of brass, having 3.81 cm. I.D., 0.3175 cm. wall thickness and for the tests at 440 Hz. the length is 38.65 cm. The three circular exhaust vents are of brass, having 0.3175 cm. wall thickness, and I.D. 1.27 cm. 2.54 cm., and 3.81 cm. (1/2", and 1", and 1 1/2" respectively). All are 3.30 cm. long. Each has a plug, machined so that when inserted the vent is closed by a surface smoothly fitting the inside surface of the main resonance tube.

Tubes with slot vents were constructed so that the annular slots have areas equal to the areas of the circular vents having I.D. 2.54 and 3.81 cm. Plugs to close the slot vent were not made, so that, as later remarks will show, the absolute values of the attenuation constants associated with these two vents could not be determined.

A particularly difficult problem to overcome was the sealing and smooth operation of the pistons. It appeared that during the first portions of this work a major source of errors and poor reproducibility of the data, was due to shifting of the average positions of the pistons. We could neither control precisely nor measure accurately the positions of the pistons. Small displacements cause measurable changes in the resonant frequency of the



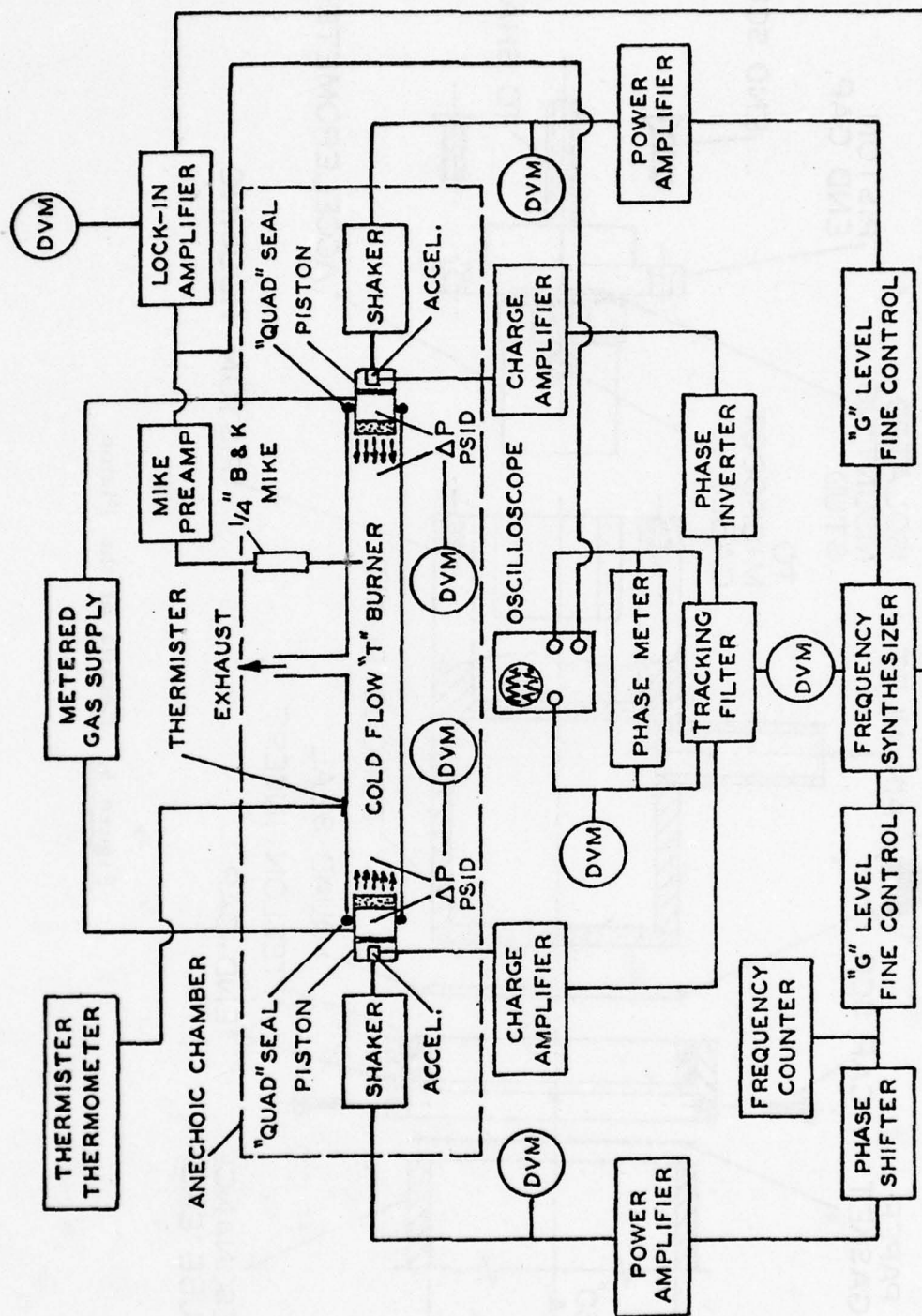


Figure 4. Schematic Diagram of the Resonance Tube and Apparatus

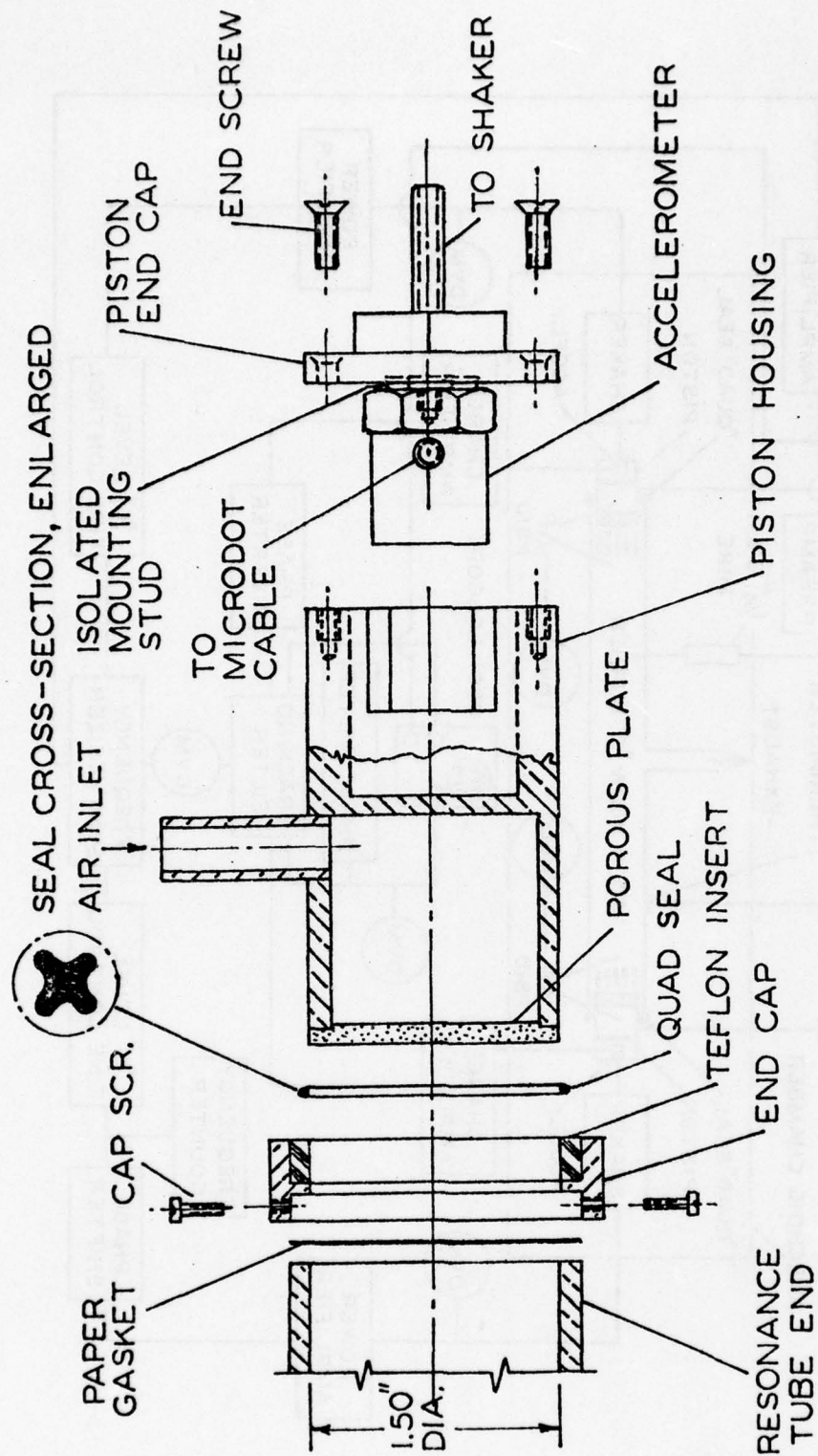


Figure 5. Details of the Piston

tube and asymmetry of the pressure field with respect to the center of the vent. Four major designs were tried. The most successful, and the one used to obtain all the data reported here, is shown in Figure 5.

Each end of the tube is fitted with a cap and a teflon insert to provide a close fit with the piston. The radial clearance is about 75 microns and is filled with silicon oil to prevent leakage. An external 'quad' seal helps to maintain alignment. The pistons are machined of aluminum with a grade 'G' porous sintered stainless steel plate 0.3175 cm. thick glued to the front, through which the flow enters. Both the amplitude and phase of the pistons are measured with accelerometers mounted close to the axis in the rear chambers of the pistons.

Coarse and fine regulators are used in series to provide the average flow from a reservoir tank which is filled from the air supply in the building. Supply pressure is monitored with Statham differential pressure gauges. Similar gauges are used to measure the pressure drop across the porous plates and therefore to maintain the desired flow rate into the tube.

The apparatus shown in Figure 4 may be best understood by considering four subsystems:

- (i) the gas supply.
- (ii) the equipment required to drive the waves.
- (iii) the instrumentation used to measure the amplitudes and relative phase of the piston motions.
- (iv) the instrumentation for measuring the waves in the tube.



The gas supply is described below in §IV. A Wavetek frequency synthesizer, Model 171, provides the signal to drive the B. & K. electromagnetic shakers, Model 4810. An amplifier, Realistic Model SA 10, is used with each of the shakers, and in series with one is a phase shifter. Thus very precise control is maintained of frequency, amplitude, and relative phase.

Each piston is fitted with an accelerometer, Endevco Model 2275; the signal is amplified by a charge amplifier, Unholtz - Dickie Model D11. Both amplified signals are filtered through a two-channel tracking filter, Spectral-Dynamics Model SD 122 with its carrier generator, Model SD 120. The relative phase of the signals is detected with a Wavetek phase meter, Model 740; the accuracy of the phase measurement is improved by including a phase inversion circuit.

All data for the pressure waves are taken with a B. & K. one-quarter inch microphone, Model 41.36. The desired signal is extracted from the noise generated by the mean flow by using a Princeton Applied Research lock-in amplifier, Model 124A. This technique has been effective up to the largest flow speeds, 4.0 ft./sec., used to date.\* The output of the lock-in amplifier is measured with a 5 1/2 digit Data Precision Digital Voltmeter, Model 3500.

During the first part of this program, some difficulties were encountered with interference from airborne noise and local reflections within the room. All of the data reported here

---

\* The highest speed for the data included here is 2.5 ft./sec. Only a few tests have been carried out at higher speeds.

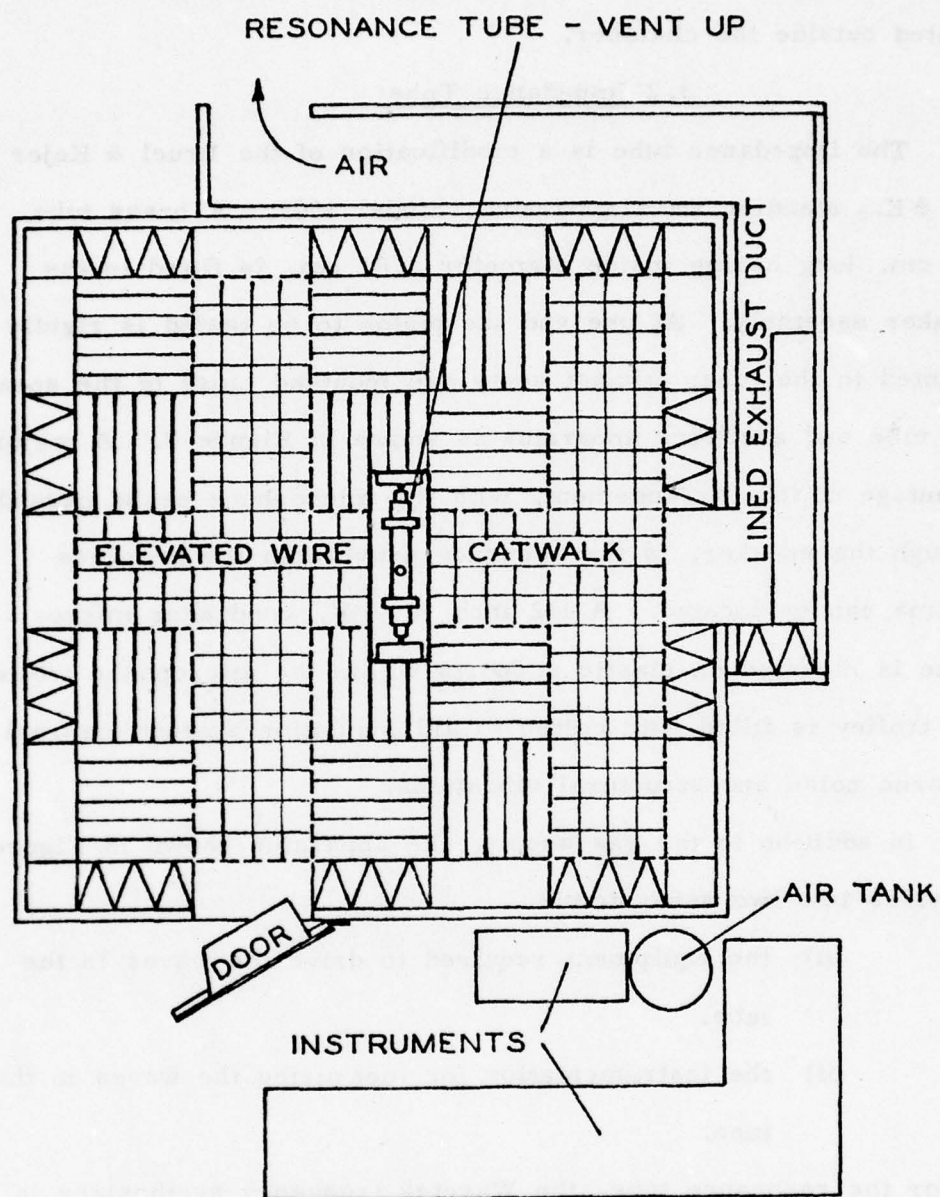


Figure 6. Anechoic Chamber  
Floor Plan Showing  
Location of Apparatus

were taken with the resonance tube placed in an anechoic chamber, as shown in Figure 6. The air supply and the instrumentation were located outside the chamber.

### 3.2 Impedance Tube

The impedance tube is a modification of the Bruel & Kejer (B. & K.) standing wave apparatus, Model 4002. A brass tube, 100 cm. long having inside diameter 3.81 cm. is fitted to the speaker assembly. At one end the piston to be tested is rigidly mounted to the tube; exhaust vents are mounted close to the speaker. The tube and ancillary apparatus is shown in Figure 7. A major advantage of this arrangement, with the microphone probe passed through the speaker, is the accuracy with which the pressure minima can be located. A 1/2 inch B. & K. condenser microphone is mounted on elastic supports within the microphone trolley. The trolley is filled with cotton to aid insulation against external airborne noise and structural vibrations.

In addition to the gas supply, the apparatus shown in Figure 8 divides into two subsystems:

- (i) the equipment required to drive the waves in the tube.
- (ii) the instrumentation for measuring the waves in the tube.

As for the resonance tube, the Wavetek frequency synthesizer is amplified with a Realistic amplifier, and excites the loudspeaker.

A 1/2 inch B. & K. measuring amplifier, Model 2607, passes through the tracking filter, and then returns to the measuring amplifier which provides a means of quickly, but approximately,



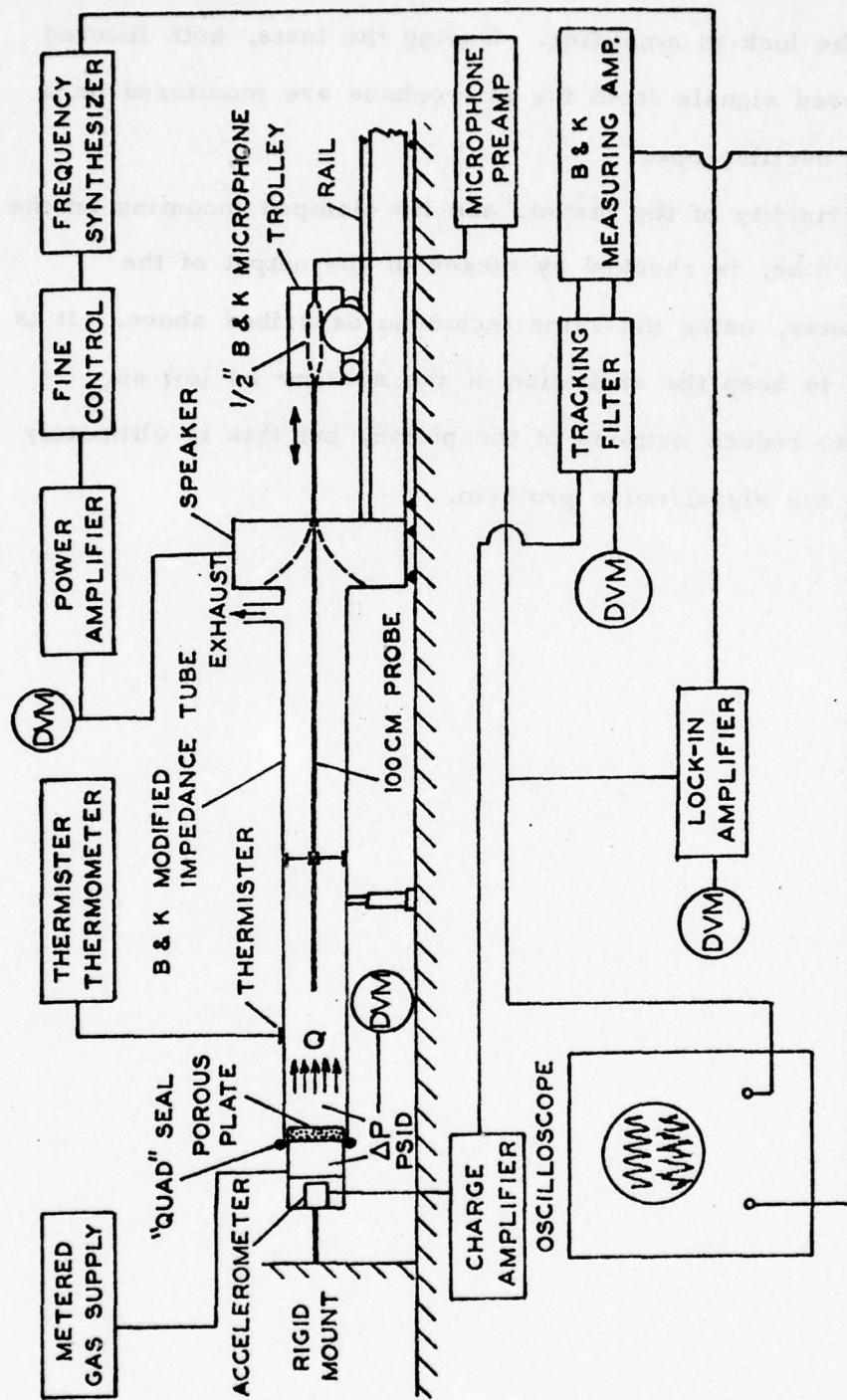


Figure 7. Schematic Diagram of Impedance Tube and Apparatus

locating the maxima and minima. Accurate results are obtained by using the lock-in amplifier. During the tests, both filtered and unfiltered signals from the microphone are monitored on a dual-beam oscilloscope.

The rigidity of the piston, and its clamped mounting on the impedance tube, is checked by means of the output of the accelerometer, using the same technique described above. It is desirable to keep the excitation of the speaker as low as possible, to reduce motions of the piston, but this is ultimately limited by the signal/noise problem.

#### IV. CALIBRATION PROCEDURES AND ESTIMATES OF ERRORS

It will be clear from the discussions in the following two sections that the quantities to be determined are small and vary relatively slowly with the Mach number of the average flow. Considerable care and good instrumentation are required to obtain the accuracy required. An important part of the work has been the attention paid to calibration of the instruments.

##### 4.1 Calibration of the Gas Supply System

Figure 8 shows the arrangement used to calibrate the porous plates. The impedance tube is used as a convenient mount for the pistons. A Brooks flowmeter (0-322 SCFM full scale) had been separately calibrated using a wet-test meter (0-100 SCFH air flow maximum). The supply pressure and flow rate are controlled and maintained constant by a series of coarse and fine pressure regulators and a fine metering needle valve. The pressure drop across the porous plate is measured with Statham differential pressure gauges (0-10 psia); the pressure gauges have been calibrated at the Standards and Calibrations Laboratory of the Jet Propulsion Laboratory.

The results, flow rate as a function of pressure drop for the two porous plates, are shown in Figure 9. These plates were chosen to provide high acoustic impedance, which implies a relatively large pressure drop for a given flow rate. The data shown in Figure 9 are within the tolerances ( $\pm 30\%$ ) quoted by the manufacturer, Pall Western Corporation.



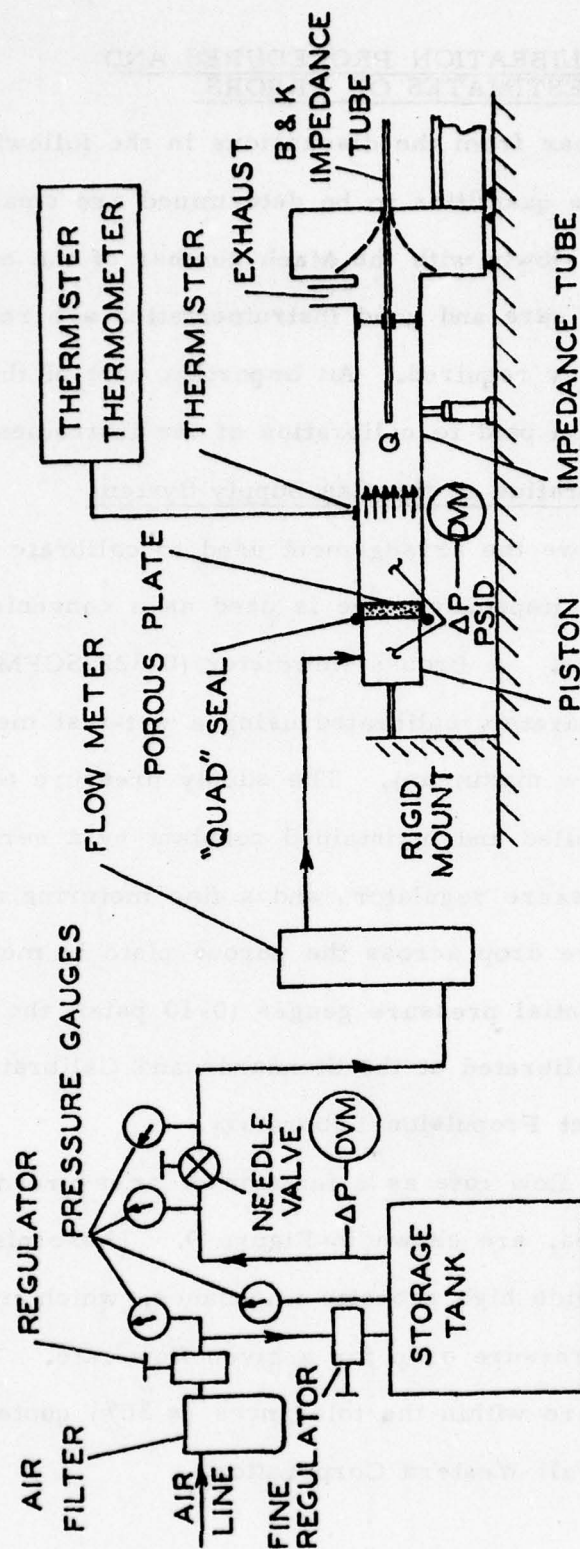


Figure 8. Flow Circuit for Calibration of Porous Plates

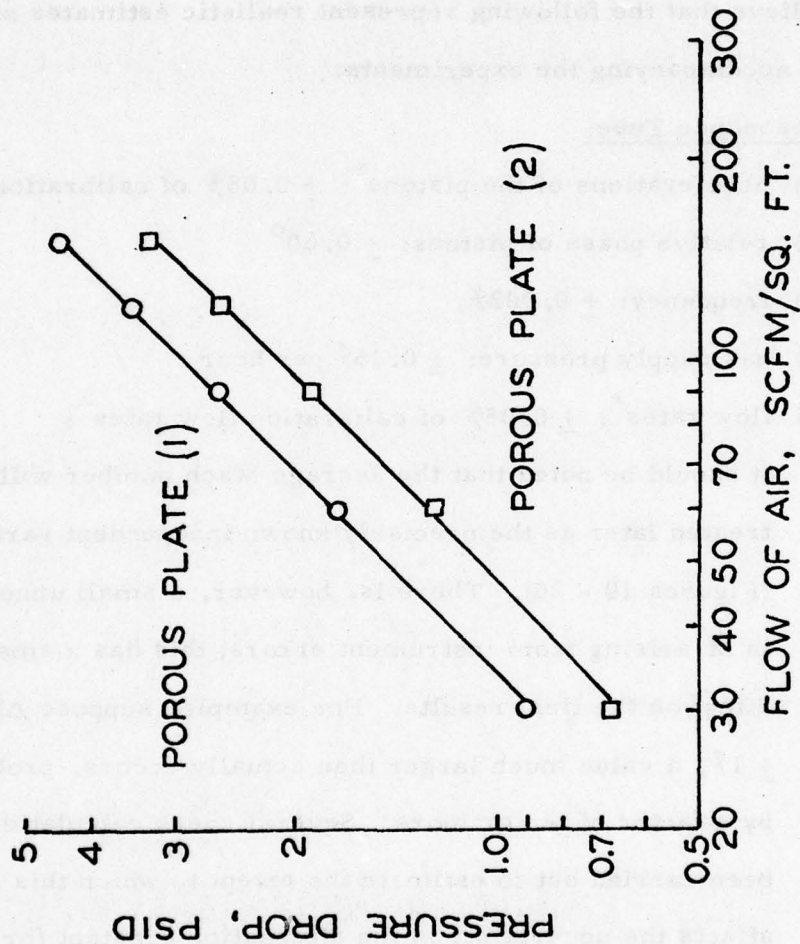


Figure 9. Data for Flow Rates Through the Porous Plates

#### 4.2 Calibration of Microphones

The values of the sensitivities and the frequency response curves of the microphones are provided by the manufacturer. Periodic verifications have been made during this work using a B. & K. piston-phone microphone calibrator, Model 4220.

#### 4.3 Sources and Estimates of Errors

We believe that the following represent realistic estimates of the errors accompanying the experiments.

##### (a) Resonance Tube

- (i) accelerations of the pistons<sup>\*</sup>:  $\pm 0.08\%$  of calibration
- (ii) relative phase of pistons:  $\pm 0.60^\circ$
- (iii) frequency:  $\pm 0.002\%$
- (iv) gas supply pressure:  $\pm 0.15\%$  per hour
- (v) flow rates<sup>\*</sup>:  $\pm 0.05\%$  of calibration flow rates<sup>\*</sup>:

It should be noted that the average Mach number will be treated later as the precisely known independent variable (Figures 10 - 20). There is, however, a small uncertainty in  $\bar{M}$  arising from instrument errors; this has a small effect on the final results. For example, suppose  $\Delta\bar{M}$  is  $\pm 1\%$ , a value much larger than actually occurs, probably by a factor of ten or more. Several check calculations have been carried out to estimate the extent to which this error affects the uncertainty in the attenuation constant for the vent. Over the range of conditions covered by this data, the uncertainties in  $\alpha_v$  are increased by a factor 1.01 - 1.07. Thus the error bars shown in



Figures 17 - 20 are only slightly increased and the qualitative conclusions in respect to the influence of the vent are unaffected.

(vi) acoustic pressure signal:  $\pm 0.10\%$ . The absolute values need not be known, for an error in the average values merely shifts the resonance curve vertically if that error is independent of frequency and amplitude for the range covered. See remarks under item (iv) for the impedance tube.

(vii) The greatest uncertainties and sources of error are associated with the end conditions at the pistons. These are due mainly to the flow through the pistons and building vibrations, both of which may produce shifts in the average position of the piston and fluctuations in the relative phase. Small changes in alignment - the axis of the piston may not be precisely aligned with the axis of the tube - can also be troublesome. Lubrication with silicon oil and the external "quad-seal" helped alleviate these problems. Without these improvements, we encountered serious difficulties with large test-to-test variations of the resonant frequency, accompanied also by changes in the pressure amplitude for the same piston motion.

(b) Impedance Tube

(i) acceleration of the piston: 0.0007g. For correct

results, the piston should be stationary. Best results were obtained after a sturdy clamp was installed to anchor the piston to the impedance tube. Excitation of the loudspeaker was kept to as low level as possible.

- (ii) Determination of the pressure minima is affected by the flexibility and mounting of the long probe. Spurious room noise also has some influence. Neither error is known. Ultimately, the major limitation is set by the signal/noise problem, primarily due to flow noise.
- (iii) spacial resolution of pressure minima:  $\pm 0.5\text{mm}$ .
- (iv) Unlike the measurements taken with the resonance tube, it is necessary for the tests with the impedance tube to know the absolute values of the pressure amplitude. The amplitude linearity of the lock-in amplifier enters in determining the absolute values of the signals; the internal calibrator of the instrument was used to estimate this error. A practical difficulty arises because we needed to measure signals ranging from 1% to 80% of the full-scale sensitivity for the amplifier. When the signal was only 1% of the full-scale sensitivity, the error in amplitude linearity was determined to be  $\pm 0.10\%$ . For signals greater than 30% of full-scale, it was impossible to detect the very small error. Measurements

of pressure minima in the impedance tube are necessarily made at the lower end of the scale, while measurements of pressure maxima and all data for the resonance tube are taken at the higher end of the scale. We estimate that the error in amplitude linearity of the lock-in amplifier produces an additional error amounting to roughly 5% of the existing error bars shown later in Figures 18 - 21. It may be noted that day-to-day temperature changes are ignored. The eventual effect on the attenuation constants is roughly 0.5%, arising from the influence on  $\kappa$  and the speed of sound. To minimize the effects of these errors, all tests have been repeated three times and the data have been treated statistically.



## V. MEASUREMENTS OF THE ADMITTANCE FUNCTIONS FOR THE POROUS PLATES

In order to achieve effective isolation of the gas supply system from the flow in the resonance tube it is necessary to use porous plates having high impedance. This means that the admittance, in particular the real part which must be determined, is small. Because  $A_b^{(r)}$  appears always multiplied by the speed of sound in Eq. (10), its contribution to the attenuation constant is substantial. Consequently, the admittance function is a relatively small quantity which must be accurately determined.

Tables 1 and 2 contain the values of the real part of the admittance function found for the two porous plates in the three series of tests; the average values; and the standard deviation all at 442.7 Hz. Tables 3 and 4 list the corresponding results found at 1345.0 Hz. The average values of the real part of the admittance function are shown in Figures 10 and 11 as functions of the average Mach number of the flow in the 3.81 cm. diameter tube. The solid lines in Figures 10 and 11 represent least squares fit to the data, assuming a linear variation of  $\alpha_v$  with  $\bar{M}$ .

Table 1. Data Taken With Impedance Tube,  
Porous Plate # 1, Frequency 442.7 Hz.

$\bar{M} \times 10^4$	$-A_b^{(r)} \times 10^2$	$-<A_b^{(r)}> \times 10^2$	$\sigma \times 10^6$
0	1.3752 1.3948 1.3947	1.3882	92
4.43	1.3570 1.3948 1.4010	1.3843	194
8.86	1.3826 1.3890 1.3960	1.3892	55
13.29	1.3837 1.3800 1.3965	1.3867	71
17.72	1.3470 1.3435 1.3868	1.3591	196
22.15	1.3494 1.3400 1.3722	1.3539	135

Table 2. Data Taken With Impedance Tube,  
Porous Plate #2, Frequency = 442.70 Hz.

$\overline{M} \times 10^4$	$-A_b^{(r)} \times 10^2$	$-\langle A_b^{(r)} \rangle \times 10^2$	$\sigma \times 10^6$
0	1.6879	1.6987	84
	1.6999		
	1.7084		
4.43	1.6914	1.7156	180
	1.7344		
	1.7210		
8.86	1.7050	1.6993	130
	1.6814		
	1.7116		
13.29	1.6227	1.6454	164
	1.6528		
	1.6608		
17.72	1.5961	1.6245	223
	1.6270		
	1.6505		
22.15	1.5893	1.6022	104
	1.6025		
	1.6147		



Table 3. Data Taken With Impedance Tube,  
Porous Plate #1, Frequency = 1345 Hz.

$\bar{M} \times 10^4$	$-A_b^{(r)} \times 10^2$	$-\langle A_b^{(r)} \rangle \times 10^2$	$\sigma \times 10^6$
0	1.4949	1.4772	135
	1.4744		
	1.4623		
4.43	1.5005	1.4881	165
	1.4989		
	1.4648		
8.85	1.5742	1.5647	69
	1.5584		
	1.5614		
13.29	1.5133	1.4995	194
	1.5133		
	1.4721		
17.72	1.5080	1.5139	123
	1.5311		
	1.5027		
22.15	1.4974	1.4904	65
	1.4922		
	1.4817		

Table 4. Data Taken With Impedance Tube,  
Porous Plate #2, Frequency = 1345 Hz.

$\bar{M} \times 10^4$	$-A_b^{(r)} \times 10^3$	$-\langle A_b^{(r)} \rangle \times 10^3$	$\sigma \times 10^4$
0	1.6454 1.6719 1.6346	1.6506	157
4.43	1.7000 1.6948 1.6985	1.6978	22
8.86	1.7011 1.7255 1.6826	1.7031	176
13.29	1.7135 1.6997 1.6870	1.7001	108
17.72	1.6478 1.6401 1.6737	1.6539	144
22.15	1.6012 1.6331 1.6296	1.6213	143

FREQUENCY 442.70 Hz

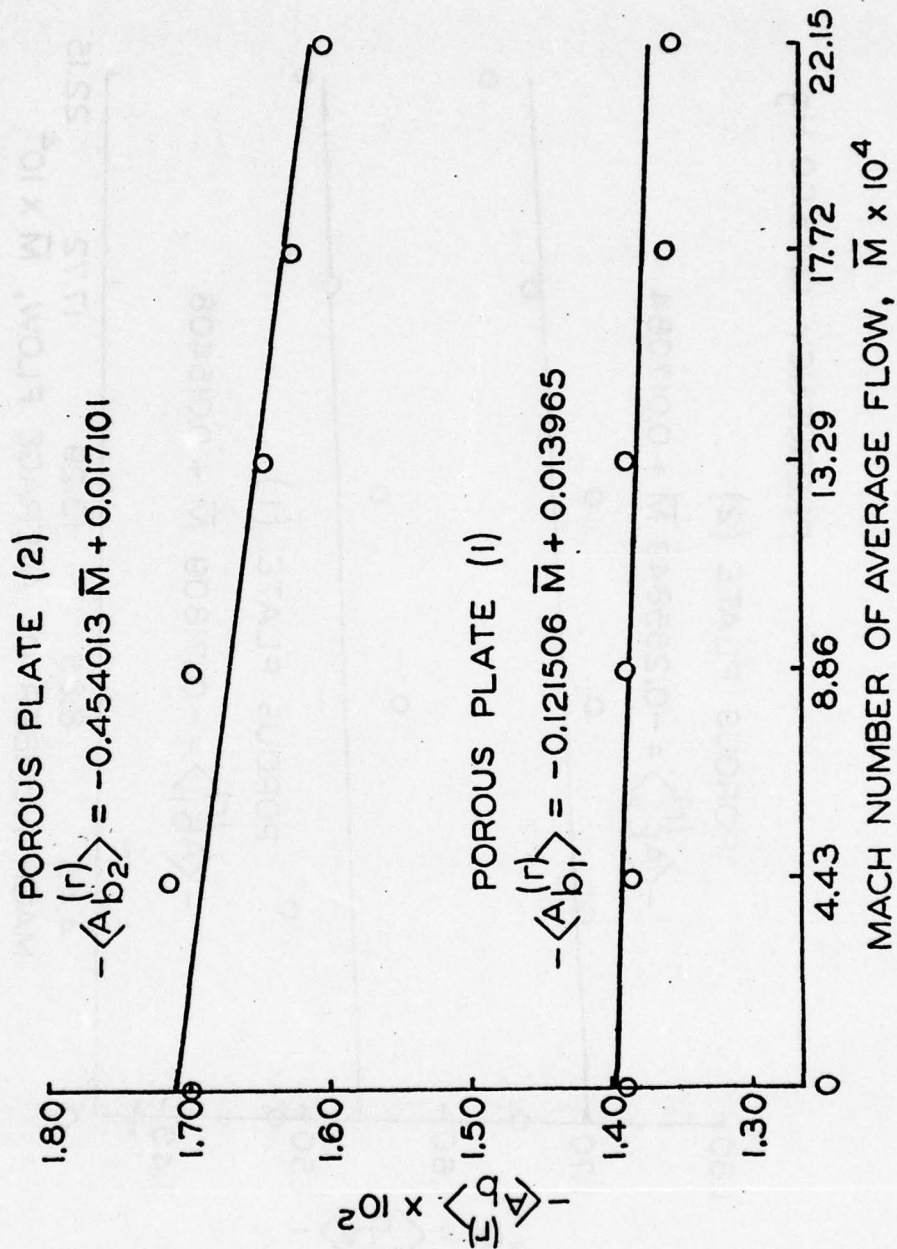


Figure 10. Measured Admittance Functions at 442.70 Hz.



FREQUENCY 1345.00 Hz.

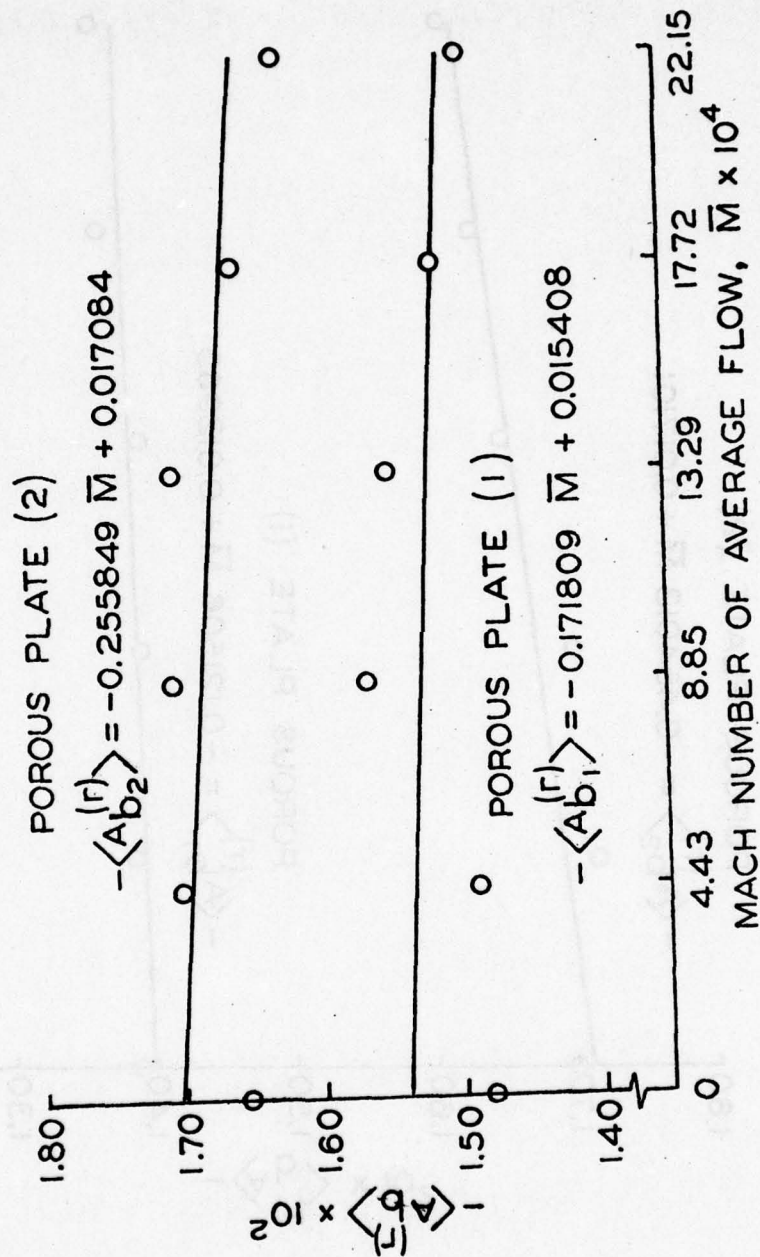


Figure 11. Measured Admittance Functions at 1345.00 Hz.

## VI. MEASUREMENTS OF THE NET ACOUSTIC LOSSES IN THE RESONANCE TUBES

The strategy to determine the influence of the exhaust vent is based on the familiar interpretation of the linear attenuation constant  $\alpha$ :

$$\alpha = \frac{1}{2} \frac{\overline{\dot{E}}}{\overline{E}} \quad (17)$$

Here  $\overline{\dot{E}}$  stands for the time-average of the rate of change of acoustic energy in the tube and  $\overline{E}$  is the time-average of the energy itself. Because the system is assumed to be linear, the net value of  $\alpha$ , as it appears in Equation (8), for example, and shown in Figure 2, may be written as the sum of contributions from various sources.

For the tests reported here we may distinguish three contributions to  $\alpha = \alpha_{\text{net}}$ :

$$\alpha_{\text{net}} = \alpha_b + \alpha_d + \alpha_v \quad (18)$$

where

$\alpha_b$ : attenuation constant associated with the boundaries at the ends, the porous plates on the pistons.

$\alpha_d$ : attenuation constant associated with acoustic radiation losses and viscous losses along the lateral boundary.

$\alpha_v$ : the attenuation constant associated with the vent.

It is  $\alpha_v$  which we wish to determine. According to the sign convention used here,  $\alpha_v$  is a negative number if the acoustic/mean flow interactions in the region of the vent produce a gain of acoustic energy.

Tables 5 - 9 contain the data taken for three series of tests performed at each Mach number for the five vents tested

at 442 Hz. Table 10 contains the data for the only vent tested at 1345 Hz. The average values and standard deviation for both the net attenuation constant and frequency are given. Note that for the circular vents, two series of tests have been carried out with no flow: one series with the vent open and one with the vent closed. The difference between the values of the attenuation constant for these two cases should represent the losses due to radiation through the vent.

Figures 12 - 17 show the average values of  $\alpha_{\text{net}}$  as a function of the average Mach number. Again the solid lines in the figures represent least-squares fits, assuming that  $\alpha_{\text{net}}$  varies linearly with the average Mach number.



Table 5.

Data Taken With Resonance Tube,  
 $\frac{1}{2}$ " Circular Vent, Frequency = 442.70 Hz.

$\bar{M} \times 10^4$	$\alpha_{\text{net}}$ ( $\text{sec}^{-1}$ )	f (Hz)	$\langle \alpha_{\text{net}} \rangle$ ( $\text{sec}^{-1}$ )	$\sigma_{\alpha}$ ( $\text{sec}^{-1}$ )	$\langle f \rangle$ (Hz)	$\sigma_f$ (Hz)
0	41.94 41.55 41.82	444.10 443.50 443.90	41.77	0.16	443.83	0.25
4.43	41.88 42.21 41.98	442.00 441.90 443.40	42.02	0.14	442.43	0.68
8.86	42.06 42.55 42.57	442.50 442.30 442.90	42.39	0.24	442.57	0.25
13.29	42.26 41.48 42.56	442.50 442.40 442.30	42.43	0.13	442.40	0.08
17.72	41.87 41.46 41.28	442.60 442.10 442.40	41.54	0.25	442.37	0.21
22.15	41.20 41.52 41.27	442.50 443.10 442.50	41.33	0.14	442.70	0.28
0 (vent closed)	41.43 41.97 41.73	443.20 443.00 443.00	41.71	0.22	443.07	0.09

Table 6.

Data Taken With Resonance Tube,  
1" Circular Vent, Frequency = 444.79 Hz.

$\bar{M} \times 10^4$	$\alpha_{\text{net}}$ ( $\text{sec}^{-1}$ )	f (Hz)	$\langle \alpha_{\text{net}} \rangle$ ( $\text{sec}^{-1}$ )	$\sigma_{\alpha}$ ( $\text{sec}^{-1}$ )	$\langle f \rangle$ (Hz)	$\sigma_f$ (Hz)
0	40.85 39.86 40.64	446.50 443.00 445.00	40.45	0.43	444.83	1.43
4.43	40.86 40.56 40.88	446.10 443.90 442.90	40.77	0.15	444.30	1.34
8.86	40.71 40.49 40.42	446.20 444.50 443.50	40.54	0.12	444.73	1.11
13.29	40.75 40.50 40.65	446.30 444.50 444.50	40.64	0.10	445.10	0.85
17.72	40.39 40.13 39.87	445.50 442.90 444.90	40.13	0.21	444.43	1.11
22.15	40.61 41.02 40.48	446.00 443.90 446.10	40.70	0.23	445.33	1.01
0 (vent closed)	40.03 39.69 39.91	444.50 444.60 443.00	39.88	0.14	442.70	1.61

Table 7. Data Taken With Resonance Tube,  
1½" Circular Vent, Frequency = 451.61 Hz.

$\overline{M} \times 10^4$	$\alpha_{\text{net}}$ (sec <sup>-1</sup> )	f (Hz)	$\langle \alpha_{\text{net}} \rangle$ (sec <sup>-1</sup> )	$\sigma_{\alpha}$ (sec <sup>-1</sup> )	$\langle f \rangle$ (Hz)	$\sigma_f$ (Hz)
0	43.02 42.36 41.78	452.30 450.10 455.10	42.39	0.51	452.50	2.05
4.43	42.74 42.34 41.52	450.80 449.50 454.60	42.20	0.51	451.63	2.15
8.86	42.31 42.07 41.19	451.20 450.00 452.00	41.86	0.48	451.07	0.82
13.29	41.86 42.00 41.50	451.60 450.00 452.00	41.79	0.21	451.20	0.85
17.72	41.72 42.27 41.27	450.90 450.20 452.90	41.75	0.41	451.33	1.14
22.15	41.47 41.26 40.84	451.40 451.00 453.40	41.19	0.26	451.93	1.05
0 (vent closed)	41.24 41.37 41.42	444.00 444.00 444.00	41.34	0.08	444.00	0.00



Table 8. Data Taken With Resonance Tube,  
1" Eq Slot Vent, Frequency = 446.72 Hz.

$\overline{M} \times 10^4$	$\alpha_{\text{net}}$ ( $\text{sec}^{-1}$ )	f (Hz)	$\langle \alpha_{\text{net}} \rangle$ ( $\text{sec}^{-1}$ )	$\alpha$ ( $\text{sec}^{-1}$ )	$\langle f \rangle$ (Hz)	$f$ (Hz)
0	41.44	444.80	41.24	0.16	447.07	1.62
	41.05	447.90				
	41.24	448.50				
4.43	41.37	445.30	41.34	0.02	446.33	0.78
	41.33	446.50				
	41.31	447.20				
8.85	41.45	445.50	41.23	0.24	446.40	0.70
	40.90	446.50				
	41.34	447.20				
13.29	40.95	446.90	41.17	0.19	447.20	0.29
	41.15	447.60				
	41.42	447.10				
17.72	41.50	445.50	41.43	0.14	446.60	1.04
	41.56	448.00				
	41.23	446.30				
22.15	41.06	446.70	41.25	0.16	446.70	0.24
	41.45	447.00				
	41.23	446.40				

Table 9.

Data Taken With Resonance Tube,  
1½" Eq Slot Vent, Frequency = 446.09 Hz.

$\overline{M} \times 10^4$	$\alpha_{\text{net}}$ (sec <sup>-1</sup> )	f (Hz)	$\langle \alpha_{\text{net}} \rangle$ (sec <sup>-1</sup> )	$\sigma_{\alpha}$ (sec <sup>-1</sup> )	$\langle f \rangle$ (Hz)	$\sigma_f$ (Hz)
0	39.46	447.80	39.70	0.28	447.20	0.85
	39.54	447.80				
	40.09	446.00				
4.43	39.69	447.30	39.63	0.17	445.77	1.16
	39.40	444.50				
	39.80	445.50				
8.86	39.63	447.50	39.52	0.10	446.00	1.08
	39.38	445.00				
	39.54	445.50				
13.29	39.47	447.70	39.43	0.13	446.27	1.01
	39.26	445.50				
	39.57	445.60				
17.72	39.26	445.20	39.13	0.14	445.83	0.59
	39.18	446.30				
	38.94	445.00				
22.15	38.99	444.90	38.95	0.25	445.47	0.73
	39.24	446.50				
	38.63	445.00				

Table 10.

Data Taken With Resonance Tube,  
 $\frac{1}{2}$ " Circular Vent, Frequency = 1340.88 Hz.

$\bar{M} \times 10^4$	$\alpha_{\text{net}}$ ( $\text{sec}^{-1}$ )	f (Hz)	$\langle \alpha_{\text{net}} \rangle$ ( $\text{sec}^{-1}$ )	$\sigma_{\alpha}$ ( $\text{sec}^{-1}$ )	$\langle f \rangle$ (Hz)	$\sigma_f$ (Hz)
0	124.13	1341.00	124.23	0.13	1341.07	0.05
	124.16	1341.10				
	124.41	1341.10				
4.43	123.79	1343.50	124.07	0.21	1343.60	0.08
	124.31	1343.60				
	124.10	1343.70				
8.86	124.22	1341.60	123.97	0.18	1341.63	0.05
	123.81	1341.60				
	123.89	1341.70				
13.29	124.05	1342.10	123.97	0.07	1342.07	0.05
	123.88	1342.10				
	123.98	1342.00				
17.72	123.98	1337.40	124.29	0.22	1337.40	0.00
	124.41	1337.40				
	124.49	1337.40				
22.15	125.84	1339.50	126.04	0.19	1339.50	0.00
	126.00	1339.50				
	126.29	1339.50				
0 (vent closed)	123.60	1340.10	123.96	0.28	1340.50	0.33
	124.29	1340.50				
	124.00	1340.90				



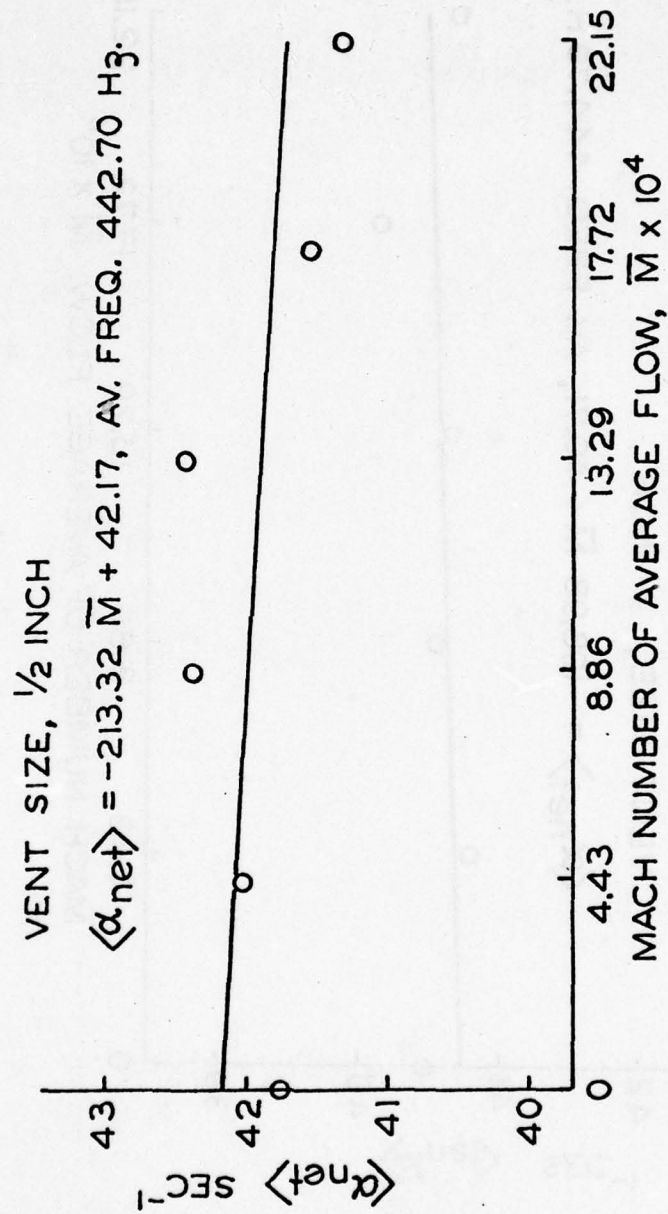


Figure 12. Net Values of Attenuation  
Constant, 1/2 inch Circular  
Vent, 442.70 Hz.

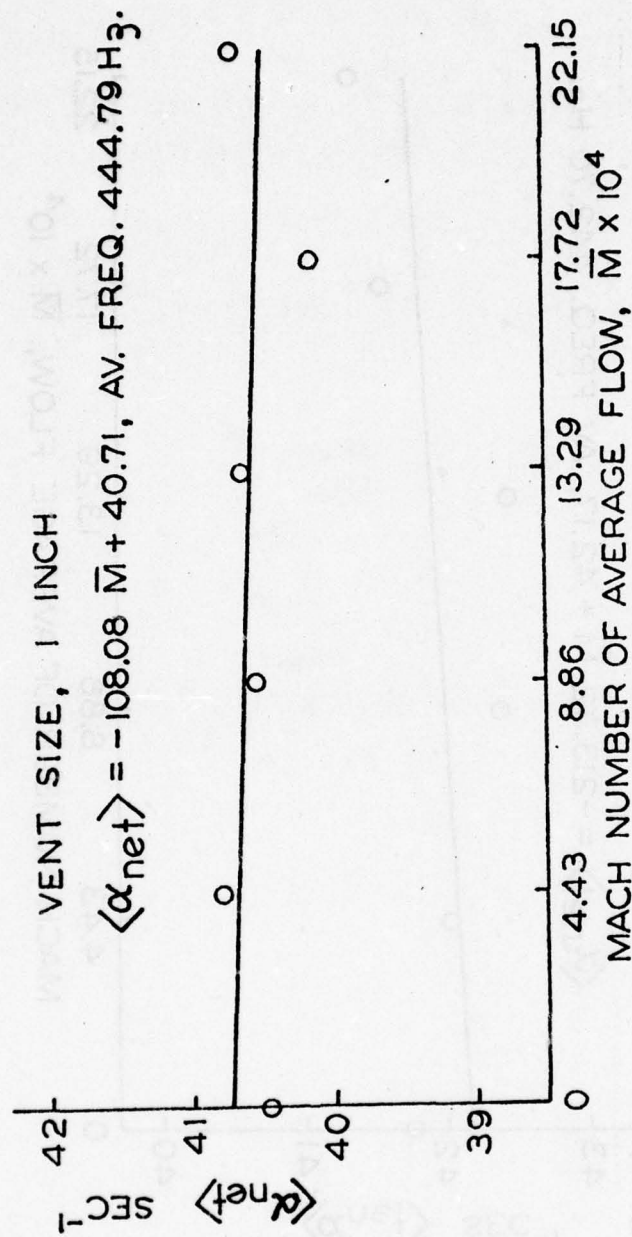


Figure 13. Net Values of Attenuation  
Constant, 1 Inch Vent, 444.79 Hz.

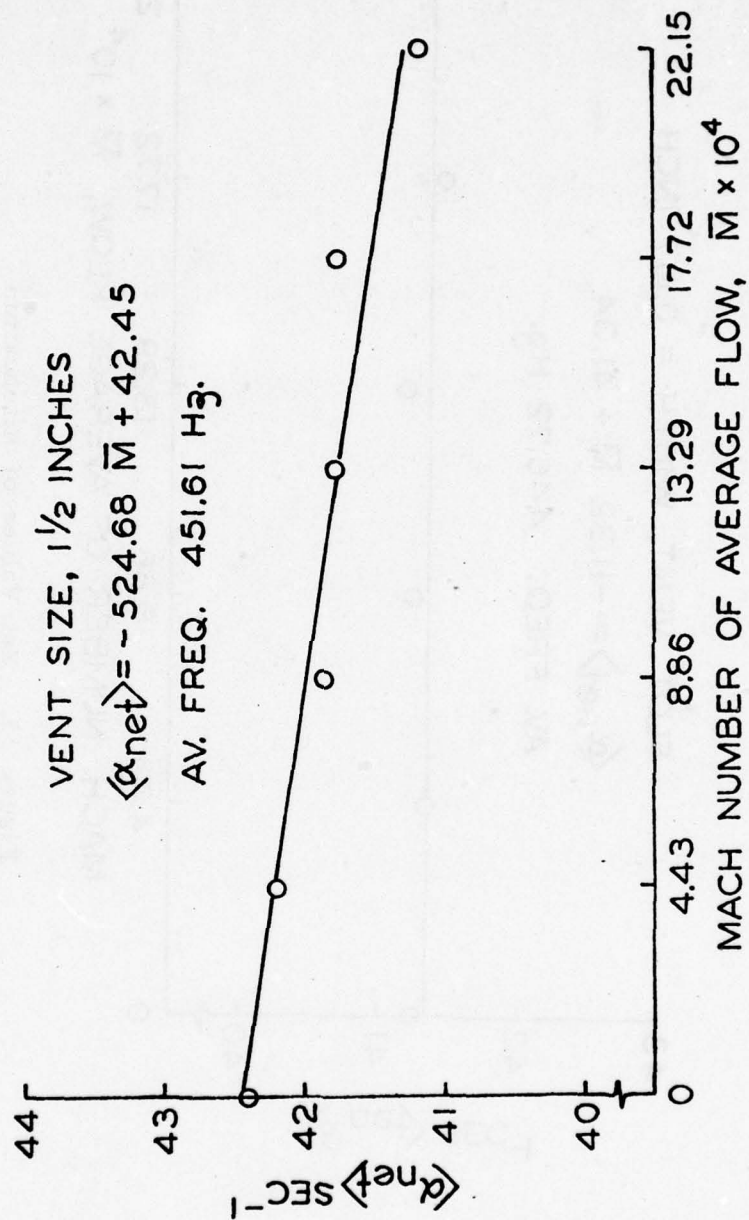


Figure 14. Net Values of Attenuation  
Constant, 1 1/2 Inch Vent, 451.61 Hz.



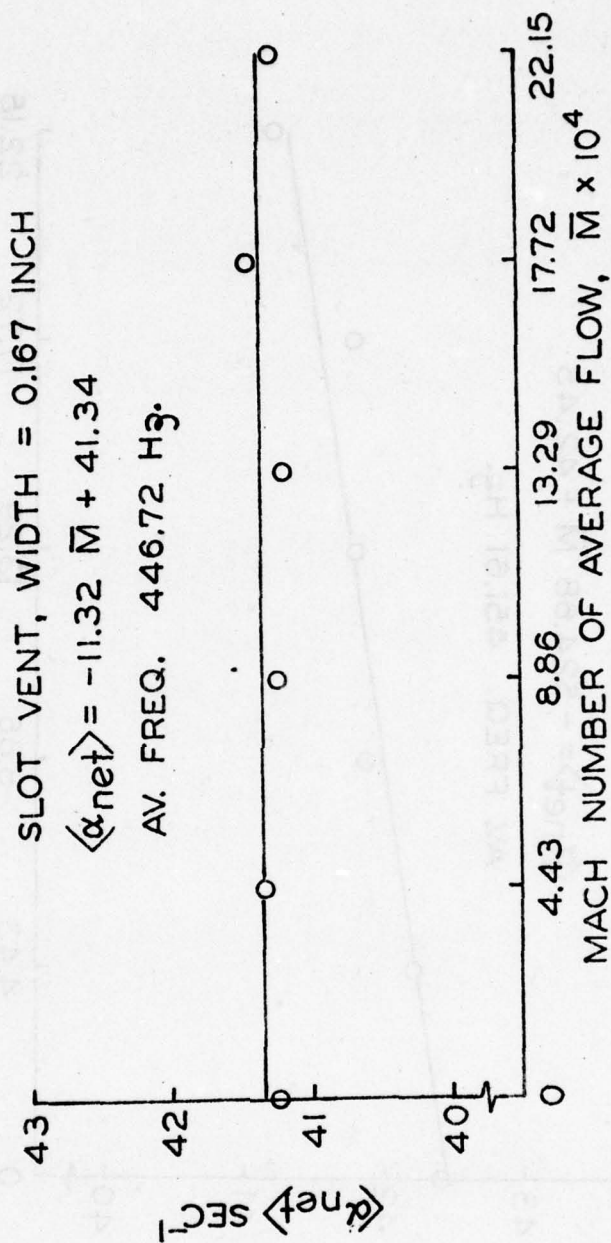


Figure 15. Net Values of Attenuation  
 Constant, 0.167 Inch Slot Vent, 446.72 Hz.

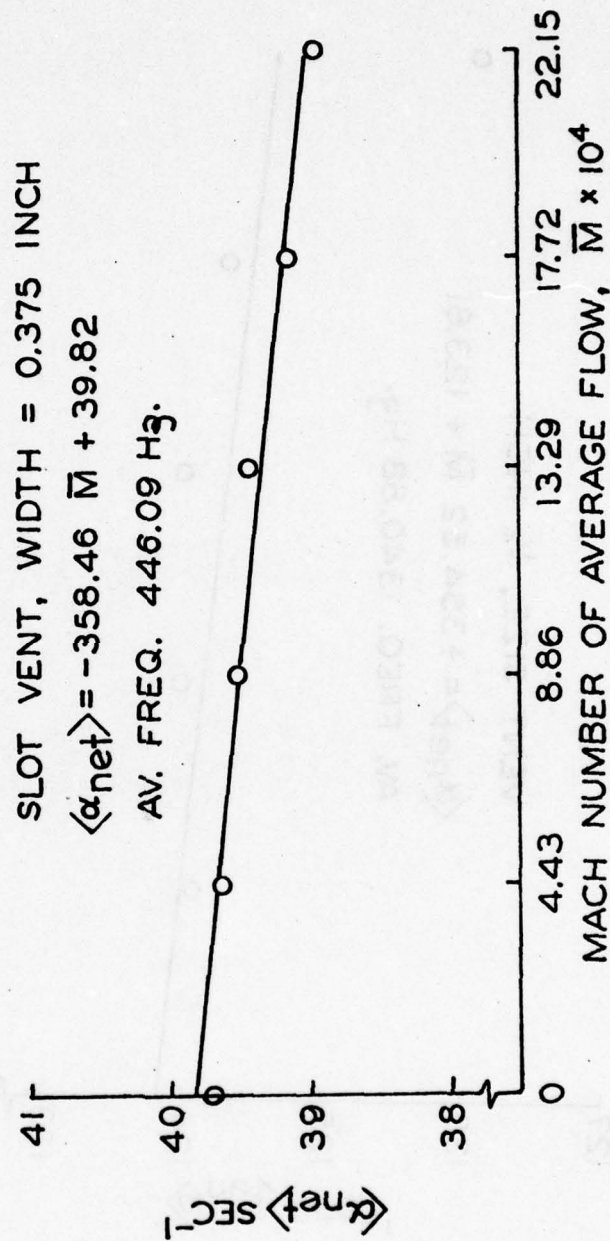


Figure 16. Net Values of Attenuation  
 Constant, 0.375 Inch Slot  
 Vent, 446.09 Hz.

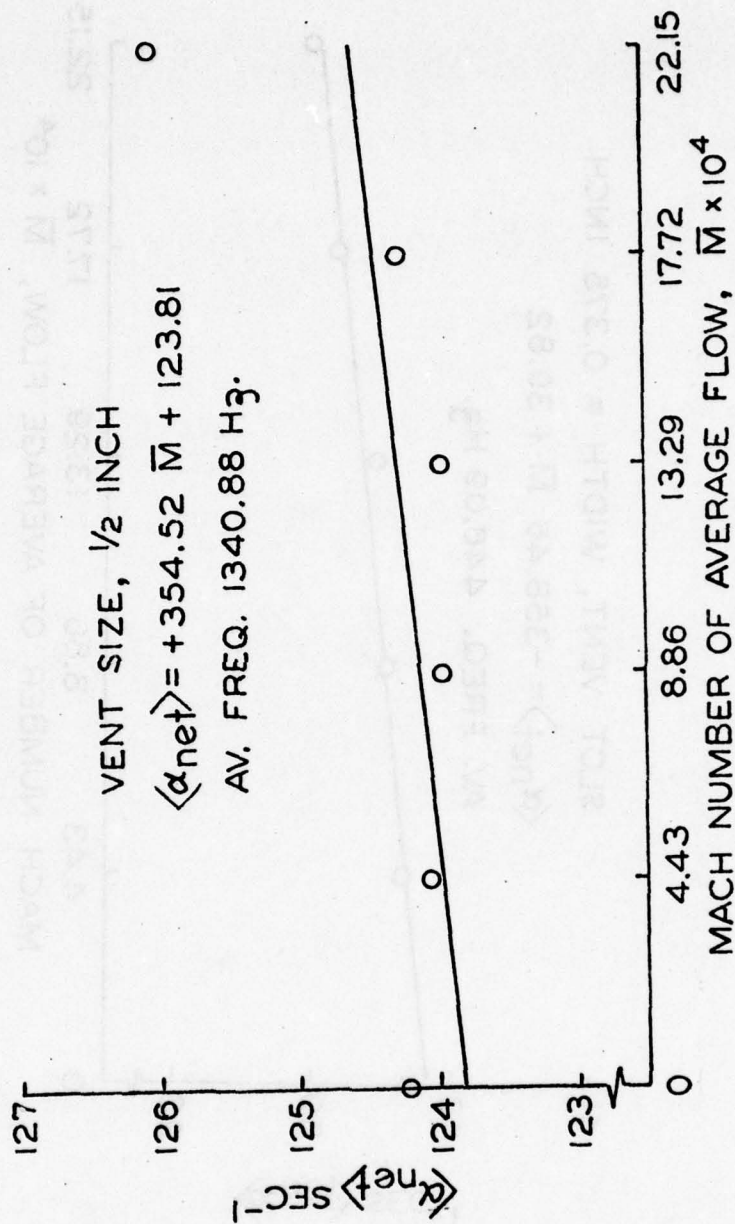


Figure 17. Net Values of Attenuation Constant, 1/2 Inch Circular Vent, 1340.88 Hz.



## VII. ANALYSIS OF THE RESULTS AND DETERMINATION OF THE INFLUENCE OF AN EXHAUST VENT

The primary purpose of the program is of course to determine the influence of the exhaust vent and to compare with the prediction deduced from the one-dimensional analysis. With the data given in § VI we are able also to find directly the radiation losses from a vent with no flow.

### 7.1 The Influence of a Vent According to the One-Dimensional Approximation

It is unnecessary to repeat here the computations leading to the theoretical result; discussions may be found in References 2, 3 and 4, Appendix G. According to Equation (G.8) of Reference 4, the contribution to the decay constant due to the vent is a gain, represented by

$$\alpha_v = - \frac{\bar{u}_b}{L} \left( \frac{S_b}{S_c} \right) \quad (20)$$

This formula has been deduced for a T-burner having cross-section area  $S_c$ , total area of burning surface  $S_b$  and average speed  $\bar{u}_b$  of the gases leaving the burning surface. For the configurations studied here,  $S_b/S_c = 2$  and  $\bar{u}_b = a_o \bar{M}$ . Because the frequency of the fundamental mode is  $f = a_o/2h$ , Eq. (19) can be written

$$\alpha_v = - 4\bar{M}f \quad (21)$$

This is the simple result we wish to check. There are three features which are important and can be examined with the data taken in this program:

- (i) the vent produces a gain ( $\alpha_v$ ) proportional to the average Mach number of the flow in

the main chamber;

- (ii) the gain is proportional to the frequency;
- (iii) the gain is independent of the shape and size of the vent.

## 7.2 Determination of Radiation Losses Through the Vent

When there is no flow,  $\alpha_v = 0$  by definition. There are two cases for which data have been taken: the vent is closed or open. Recall that the vent is closed with a plug machined so that the internal boundary of the resonance tube is a smooth cylinder with no opening. The values of  $\alpha_b$ , Eq. (18), are the same for the two cases but the values of  $\alpha_d$  differ by an amount due to radiation through the open vent. Hence, from the results for the net attenuation constant,

$$\begin{aligned} (\alpha_{\text{net}})_{\text{open}} - (\alpha_{\text{net}})_{\text{closed}} &= (\alpha_d)_{\text{open}} - (\alpha_d)_{\text{closed}} \\ &= \alpha_{\text{rad}} \end{aligned} \quad (22)$$

The average values, for the three series of tests conducted for each vent, can be calculated directly with Eq. (20). Let  $(\bar{\quad})$  denote the average value, and the standard deviation for  $N$  tests ( $N = 3$  here) is found from the formula

$$\begin{aligned} \sigma_{\text{rad}}^2 &= (\alpha_{\text{rad}} - \bar{\alpha}_{\text{rad}})^2 = \sigma_{\text{open}}^2 + \sigma_{\text{closed}}^2 \\ &\quad - \frac{2}{N} \sum_{i=1}^N (\alpha_{\text{open}} - \bar{\alpha}_{\text{open}})(\alpha_{\text{closed}} - \bar{\alpha}_{\text{closed}}) \end{aligned} \quad (23)$$

The results are given in Table 11 for the three circular vents. Because we did not have a means for plugging the slot vents, the corresponding results cannot be deduced from our data. As expected, the radiation losses are indeed very small.

**TABLE 11. Attenuation Constant Due to Radiation of Acoustic Energy From Circular Exhaust Vents.**

Vent Diameter (cm.)	$\langle \alpha_{\text{rad}} \rangle$ sec <sup>-1</sup>	$\sigma_{\text{rad}}$ sec <sup>-1</sup>
1.27	0.06	0.38
2.54	0.57	0.29
3.81	1.05	0.58



### 7.3 Internal Consistency of the Data and Losses Through the Lateral Boundary

We consider here the case when the vent is closed, and there is of course no average flow. Equation (18) becomes

$$\alpha_{\text{net}} = \alpha_b + \alpha_d \quad (24)$$

The question examined here is - how nearly is this equation satisfied by experimental results? From the data taken with the impedance tube,  $\alpha_b$  can be calculated from the formula given by the second term in Equation (10):

$$\alpha_b = 4f A_b^{(r)} \quad (25)$$

Hence, assuming that for each series of tests the frequency is constant (the error  $\Delta f$  being negligible compared with other errors), Equation (24) can be written to show explicitly the average values with standard deviations:

$$\langle \alpha_d \rangle \pm \Delta \alpha_d = (\langle \alpha_{\text{net}} \rangle \pm \Delta \alpha_{\text{net}}) - 4f (\langle A_b^{(r)} \rangle \pm \Delta A_b^{(r)}) \quad (26)$$

Note that, for example,  $\Delta x$  stands for the standard deviation  $\sigma_x$  associated with the quantity  $x$ .

Now the last equation could be used to find the losses represented by  $\alpha_d$ , mainly viscous losses at the boundary and other losses at joints in the hardware and radiation due to structural vibrations. For many years there have been doubts concerning the accuracy of the classical result (13) for losses due to viscous shear and heat conduction in an acoustic boundary layer. Experimental results, for example Reference 7, in-

7. Henderson, M.C., and Donnelly, G.J., "Acoustic Resonance Tube for High Pressures and Low  $f/p$ " J. Acoust. Soc. Amer. V. 34, No. 6 (June 1962) pp. 779 - 784.

evitably were larger by roughly 10% than those predicted by the formula (13). However, recent very careful work reported in Reference 8 has produced measured values within less than 1% of the theoretical values. We shall therefore assume that Equation (13) is correct, and ignore any errors associated with losses in the acoustic boundary layer. Equation (24) now becomes

$$(\alpha_d > \pm \Delta \alpha_d)_{\substack{\text{other} \\ \text{losses}}} = (\alpha_{\text{net}} > \pm \Delta \alpha_{\text{net}}) - 4f(\alpha_b^{(r)} > \pm \Delta \alpha_b^{(r)}) - \kappa a_o \quad (27)$$

Table 12 summarizes the numerical values for the three circular vents. Again, we cannot treat the slot vents because we have no provision for closing them flush with the internal lateral boundary of the resonance tube.

It is apparent from the results shown in Table 12 that the "other losses" constitute approximately 10% - 22% of the total losses in the system, varying from 1.4 sec<sup>-1</sup> for the 2.54 cm. vent to 3.2 sec<sup>-1</sup> for the 1.27 cm. vent. This conclusion demonstrates very strikingly the improvements in the apparatus and experimental techniques which have been achieved since the earlier report, Reference 1. At that time the corresponding contribution was 87 sec<sup>-1</sup>, a factor of 30-50 larger. There is no single reason why such improvements have been possible: all modifications to the resonance tubes, the impedance tube and the instrumentation have contributed.

- 
8. Quinn, T. J., Colclough, A.R. and Chandler, T.R.D.  
 "A New Determination of the Gas Constant by an Acoustical Method" Phil. Trans. V. 283 (Nov. 1976) pp. 367 - 420.

**TABLE 12. Verification Of The Data For  
Circular Vents With No Flow.  
(Vent Closed) Frequency = 442.70 Hz.**

Vent Diameter (cm.)	1.27	2.54	3.81
$\langle \alpha_{\text{net}} \rangle (\text{sec}^{-1})$	41.71	39.88	41.34
$\Delta \alpha_{\text{net}} (\text{sec}^{-1})$	0.22	0.14	0.08
$\langle A_b^{(r)} \rangle \times 10^2$	1.5435	1.5435	1.5435
$\Delta A_b^{(r)} \times 10^6$	88	88	88
$\kappa \alpha_b (\text{sec}^{-1})$	11.17	11.17	11.17
$\langle \alpha_d \rangle$ other losses	3.21	1.38	2.84
$(\Delta \alpha_d)$ other losses	0.38	0.30	0.24



#### 7.4 Determination of the Attenuation Constant for the Exhaust Vents

We shall present the results for the influence of the vent in two ways:

- (i) data for  $\alpha_v$  as a function Mach number
- (ii) calculation of the slope  $d\alpha_v/d\bar{M}$  from the data

On the basis of the remarks given in §4.3, the average Mach number is taken to be known precisely,  $\Delta\bar{M} = 0$  everywhere, and is the independent variable. Equation (18), written to show average values and uncertainties, gives

$$(\langle \alpha_v \rangle \pm \Delta \alpha_v) = (\langle \alpha_{\text{net}} \rangle \pm \Delta \alpha_{\text{net}}) - 4f \left\{ (\langle A_b^{(r)} \rangle \pm \Delta A_b^{(r)}) + \bar{M} \right\} - (\langle \alpha_d \rangle \pm \Delta \alpha_d) \quad (28)$$

The formula for  $\alpha_b = 4f(A_b^{(r)} + \bar{M})$  has been established in References 2 and 4. Also, in accord with the discussion of errors in §4.3, the error in the frequency is ignored; all contributions depending on  $\Delta f$  are negligibly small. For  $\langle A_b^{(r)} \rangle$  and  $\Delta A_b^{(r)}$  we use the average of the values for the two porous plates.

All of the necessary data have been given to evaluate the right hand side of (26) and to construct Table 13 for the three circular vents. These results are plotted as the circles with error bars in Figures 18 - 20. All three cases show the obvious trends that the vent provides a gain of acoustic energy which increases with the average Mach number. The corresponding results cannot be obtained for the slot vents because the values of  $\alpha_v$ , the radiation losses, for no flow could not be determined, as remarked above.

The solid straight lines in Figures 18 - 22 represent

the equation  $\langle \alpha_v \rangle = \langle \alpha_v(0) \rangle + \bar{M} d\langle \alpha_v \rangle / d\bar{M}$ . The derivative is computed from Equation (28) written in the form corresponding to (27)

$$\frac{d\langle \alpha_v \rangle}{d\bar{M}} \pm \Delta \left( \frac{d\langle \alpha_v \rangle}{d\bar{M}} \right) = -4f \left\{ \frac{d\langle A_b^{(r)} \rangle}{d\bar{M}} \pm \Delta \left( \frac{d\langle A_b^{(r)} \rangle}{d\bar{M}} \right) + 1 \right\} + \frac{d\langle \alpha_{net} \rangle}{d\bar{M}} \pm \Delta \left( \frac{d\langle \alpha_{net} \rangle}{d\bar{M}} \right) \quad (29)$$

We assume that  $\alpha_d$  is independent of the average Mach number. The standard deviations for the slopes have been calculated according to the technique discussed in Ref. 9, for example. For simplicity we assume also that all quantities vary linearly with the average Mach number. Table 14 is a list of the slopes of  $\alpha_v(\bar{M})$  and standard deviations, for the five vents tested at 442.7 Hz.

Although the data for the slot vents cannot be plotted in the same way as those for the circular vents, because the values of  $\langle \alpha_v \rangle$  for  $\bar{M} = 0$  are not known, it is clear from Table 14 that the slopes are quite close.

For  $f = 442.7$  Hz., the value of the slope  $d\langle \alpha_v \rangle / d\bar{M}$ , according to Equation (20), is  $-1770.80 \text{ sec}^{-1}$ . This prediction of the one-dimensional analysis is shown as the dashed lines in Figures 18 - 20; the value of  $\alpha_v = 0$  has been used for  $\bar{M} = 0$ .

Figure 21 shows the corresponding results for the single vent tested at the higher frequency 1345.00 Hz. For reasons which we do not fully understand, the data was more difficult

---

9. Young, H.D. Statistical Treatment of Experimental Data, McGraw - Hill Book Co., Inc. (New York), 1962, pp 122 ff.

to reproduce and the uncertainties are larger. The values of  $d\bar{\alpha}_v/d\bar{M}$  and the standard deviation are

$$\frac{d\langle\alpha_v\rangle}{d\bar{M}} = -3875.08 \text{ sec}^{-1}; \Delta \frac{d\langle\alpha_v\rangle}{d\bar{M}} = 1309.10 \text{ sec}^{-1}$$

For  $f = 1345 \text{ Hz.}$ , the slope  $d\langle\alpha_v\rangle/d\bar{M}$ , according to Eq. (20), is  $-5380 \text{ sec}^{-1}$ .

The data plotted in Figures 18 - 22 all show marked deviations from the linear correlation used here. We have of course chosen the linear fit because that is the form deduced with the one-dimensional correlation. We have not tried any nonlinear correlation, and we do not have a persuasive explanation for the behavior found.

An obvious possibility is that three-dimensional viscous effects exert a significant influence. We should first note that the assumption, explicit in the one-dimensional calculation, that no acoustic energy flows through the vent, is likely valid in any case. The problem to be addressed is: how are the acoustical motions destroyed in the region at the entrance of the vent? Within the one-dimensional analysis leading to the formula (20), the motions are destroyed by interactions between the acoustic and average flow fields. Part of those processes are viscous effects and are accompanied by an increase of entropy, but the viscosity coefficient, for example, is not explicit in the analysis. In addition, there may be important viscous effects associated with the flow around the relatively sharp corner at the entrance to the vent. Put another way, the wall in this region may exert forces on the flow.



If one assumes that the force exerted by the boundary is sufficient to bring the acoustical motions to rest, then this represents the maximum influence of viscous effects. In this limiting case, one finds that this loss exactly compensates the gain represented by eq. (20), and the net effect of the vent vanishes,  $\alpha_v = 0$ . This result suggests that if the observations lie above the prediction according to the one-dimensional analysis, then the difference may be attributed to the sort of viscous actions just noted, but acting incompletely.

On the other hand, there are cases (see Figures 19 - 21) in which the measurements show a greater gain than predicted with eq. (20). There seems to be no simple way to explain this behavior, aside from the obvious possibility of unknown experimental error.

**TABLE 13.** Values of the Average Attenuation Constant and Standard Deviation for Three Circular Vents.  
(Frequency = 442.7 Hz.)

Vent Diameter (cm.)	1.27		2.54		3.81	
$\bar{M} \times 10^4$	$\langle \alpha_v \rangle$ (sec <sup>-1</sup> )	$\Delta \alpha_v$ (sec <sup>-1</sup> )	$\langle \alpha_v \rangle$ (sec <sup>-1</sup> )	$\Delta \alpha_v$ (sec <sup>-1</sup> )	$\langle \alpha_v \rangle$ (sec <sup>-1</sup> )	$\Delta \alpha_v$ (sec <sup>-1</sup> )
0	+0.06	0.70	+0.57	0.89	+1.05	0.91
4.43	-0.59	0.85	-0.01	0.78	-0.04	1.08
8.86	-0.90	0.78	-0.92	0.58	-1.06	0.88
13.29	-1.15	0.72	-1.11	0.61	-1.35	0.93
17.72	-2.39	1.00	-1.97	0.88	-1.77	0.82
22.15	-3.15	0.73	-1.95	0.74	-2.36	0.86

Note on Sign Convention: Negative Values correspond to energy gain.

**TABLE 14. Slopes and Standard Deviation of the Attenuation Constant for Five Exhaust Vents. (Frequency = 442.7 Hz.)**

Circular Vents	$\frac{d\langle\alpha_v\rangle}{dM}$ (sec <sup>-1</sup> )	$\Delta\left(\frac{d\langle\alpha_v\rangle}{dM}\right)$ (sec <sup>-1</sup> )
1.29 cm.	-1474.56	333.02
2.54 cm.	-1369.31	252.03
3.81 cm.	-1785.91	196.57
Slot Vents		
(2.54)	-1272.57	184.97
(3.81)	-1619.69	171.95

**Note:** The slot vents have open areas equal respectively to circular vents having diameters 2.54 cm. and 3.81 cm.



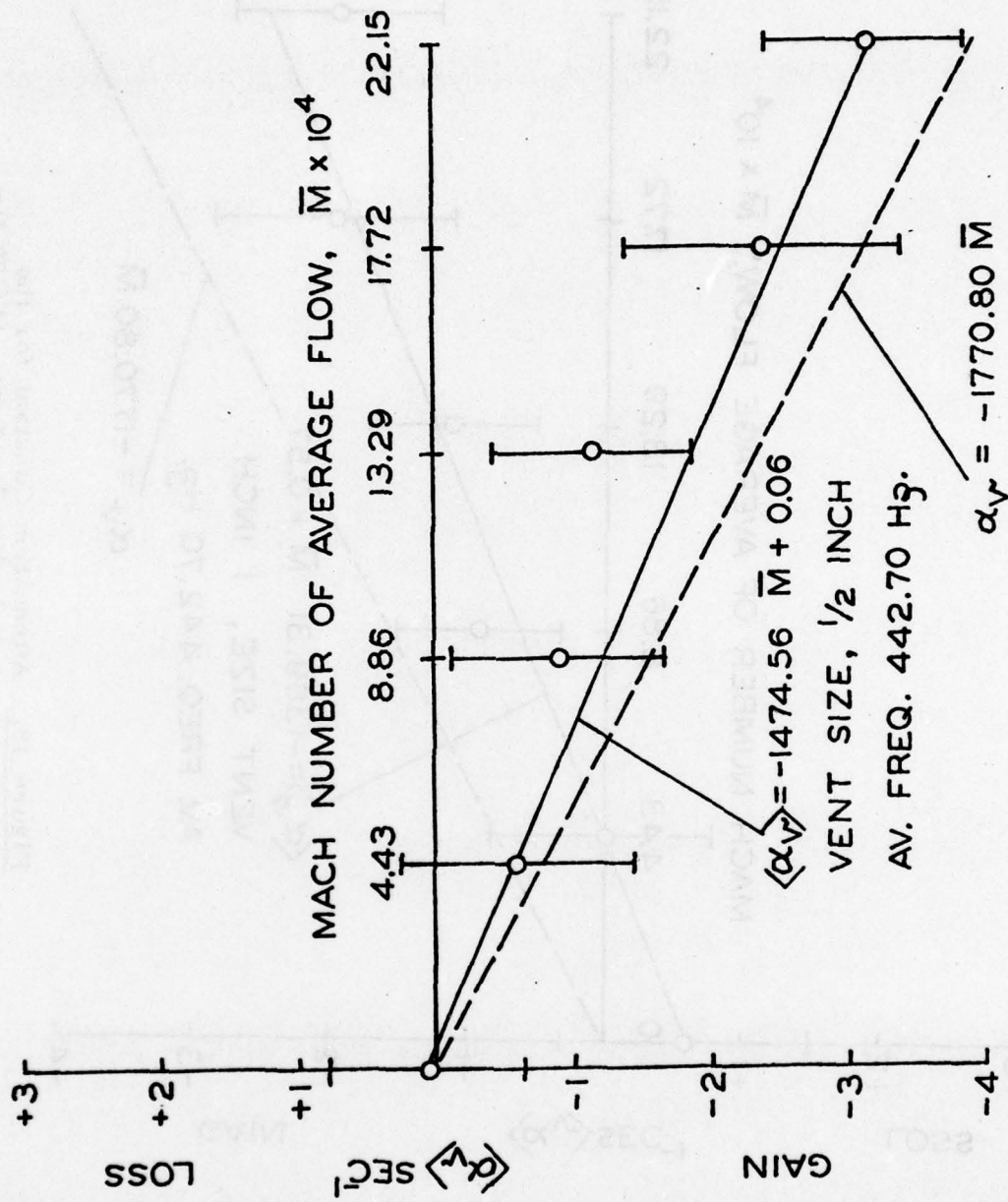


Figure 18. Attenuation Constant for the 1/2 Inch Circular Vent, 442.70 Hz.

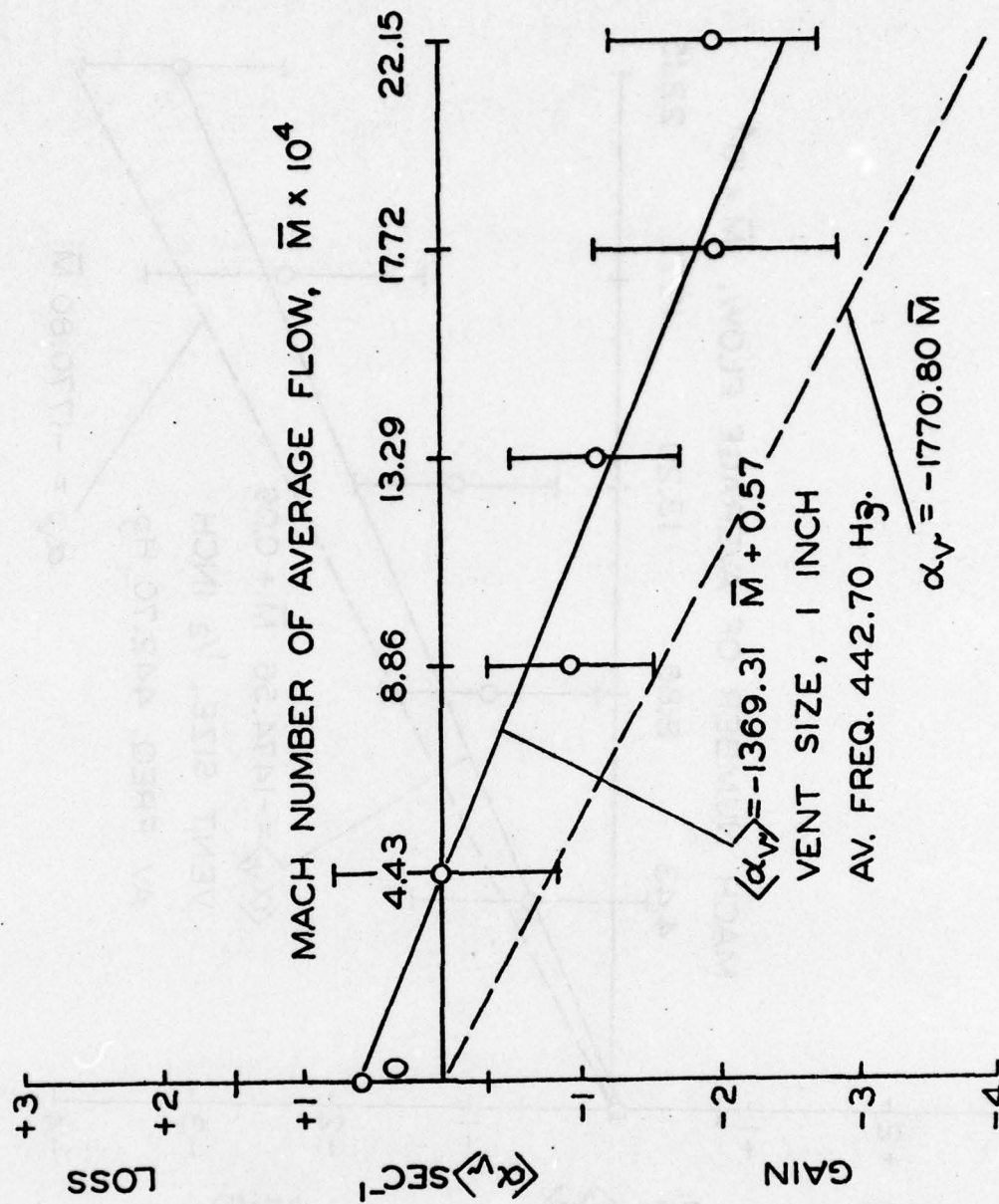


Figure 19. Attenuation Constant for the  
1 Inch Circular Vent, 442.70 Hz.

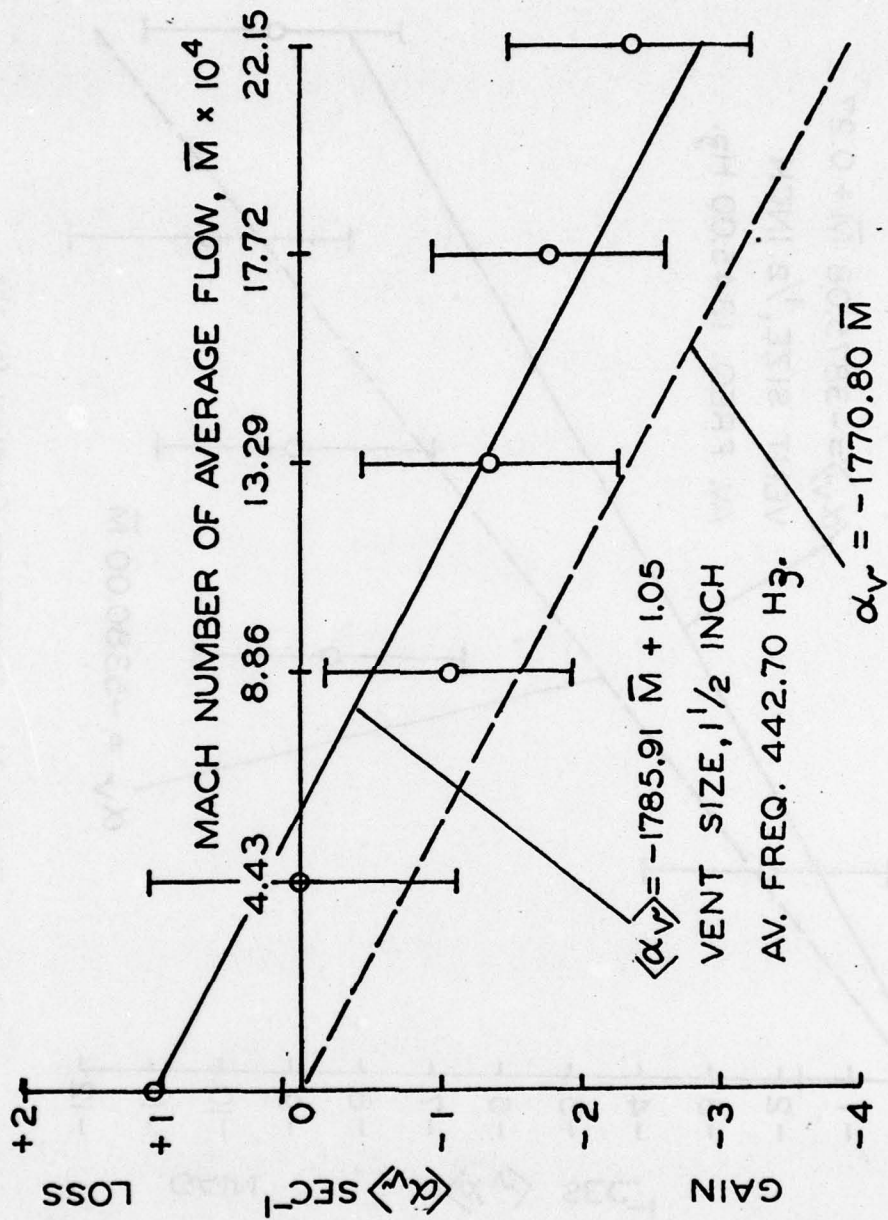


Figure 20. Attenuation Constant for the  
1 1/2 Inch Circular Vent, 442.70 Hz.



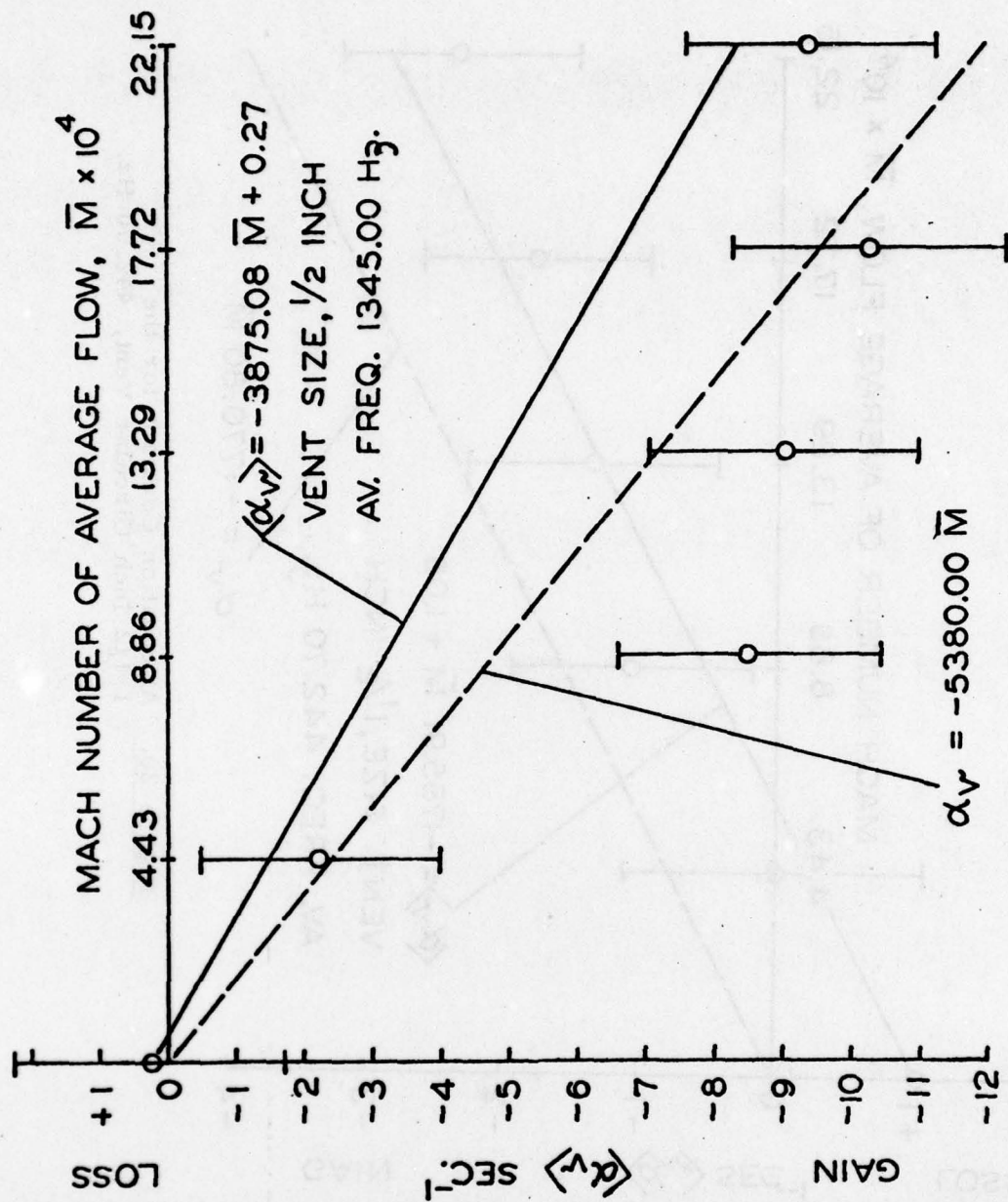


Figure 21. Attenuation Constant for the  
 1/2 Inch Circular Vent, 1345.00 Hz.

### VIII. CONCLUDING REMARKS

The most significant result of this work is the experimental demonstration that a subsonic exhaust vent in the lateral boundary of a T-burner provides a gain of acoustic energy. For all cases tested, the gain of acoustic energy increases approximately linearly with the Mach number, as predicted by the one-dimensional analysis. The one-dimensional result gives values for the growth coefficient within roughly 30% of those measured, and the three main features of the theoretical behavior have been verified: the subsonic vent produces a gain proportional to the average Mach number; proportional to the frequency; and independent of the shape. Most tests have been carried out at a frequency of approximately 446 Hz. One series (see Table 10) has been performed at 1340 Hz.: the results do verify the dependence of the gain constant on frequency. Further data will be obtained at different frequencies - and with different vents to provide more substantial bases for this conclusion.

By far most of the effort in this program has been devoted to improving the precision of the measurements. Much has been achieved simply with the acquisition of better instrumentation. But very significant changes have been made in the design of the apparatus and in experimental procedures. The results - especially when compared with those obtained during the first part of this work (Ref. 1) - demonstrate strikingly the care that is required in this sort of testing.

This is not to suggest that comparable precision is required to perform tests with burning propellants, although the

greatest possible accuracy is obviously desirable. The fundamental purpose of experiments with acoustics at ambient temperatures, such as those described here, is to establish the validity of those theoretical results which are purely acoustical. Then when tests involving combustion are carried out, the acoustical aspects of the problem are known well. One is then freed to concentrate on the truly unknown contributions associated with the combustion processes. In particular, the influence of the vent has been a serious source of uncertainty in the interpretation of data taken with the T-burners (Ref. 4). It appears now that that part of the problem has been clarified, and that data taken with T-burners should be treated accordingly.

That the contribution from the vent may be important is easily perceived. The values for  $\alpha_v$  found here are quite small, less than  $5 \text{ sec}^{-1}$ , because we have used rather small total mass flow. In T-burners based on the variable-area method of testing (see Ref. 4), the area of burning surface, and therefore the total mass flux, may be 5-10 times larger than the values used here. Consequently, according to Eq. (20), the values of  $\alpha_v$  may be 5-10 times larger, 20-50  $\text{sec}^{-1}$ . But the net values of the growth constant observed in T-burner testing are commonly in this range. The contribution of the vent is therefore obviously an important consideration.



## IX. REFERENCES

1. Culick, F.E.C. and Magiawala, K., "Measurements of Energy Losses Associated With Interactions Between Acoustic Waves and a Steady Flow Field," Final Report, Contract No. F04611-75-C-0010, AFRPL Report TR-76.
2. Culick, F.E.C., "The Stability of One-Dimensional Motions in a Rocket Motor," Comb. Sci. and Tech., V. 7 (1973), pp. 165-175.
3. Culick, F.E.C., "Remarks on Entropy Production in the One-Dimensional Approximation to Unsteady Flow in Combustion Chambers," Comb. Sci. and Tech., V. 15 (1977), pp. 93-97.
4. Culick, F.E.C. (Ed.), "T-Burner Testing of Metallized Propellants," AFRPL Report Tr-74-28 (Oct. 1974).
5. Culick, F.E.C., "Nonlinear Behavior of Acoustic Waves in Combustion Chambers," Daniel and Florence Guggenheim Jet Propulsion Center, California Institute of Technology, Pasadena, California (April 1975).
6. Morse, P.M., Vibration and Sound (2nd Edition), McGraw-Hill Book Company, New York (1948), pp. 242 ff.
7. Henderson, M.C., and Donnelly, G.J., "Acoustic Resonance Tube for High Pressures and Low  $f/p$ ," J. Acoust. Soc. Amer., V. 34, No. 6 (June 1962), pp. 779-784.
8. Quinn, T.J., Colclough, A.R. and Chandler, T.R.D., "A New Determination of the Gas Constant by an Acoustical Method," Phil. Trans., V. 283 (Nov. 1976).

References (cont.)

9. Young, H.D., Statistical Treatment of Experimental Data,  
McGraw-Hill Book Co., Inc. (New York), 1962, pp. 122 ff.